ISTANBUL TECHNICAL UNIVERSITY ★ ENERGY INSTITUTE

AB-INITIO MODELLING OF OXYGEN REDUCTION REACTION ON DOPED GRAPHENE SURFACE IN ACIDIC MEDIA

M.Sc. THESIS

Hasan Ozan AVCI

Energy Science and Technology Division

Energy Science and Technology Programme

JULY 2019

ISTANBUL TECHNICAL UNIVERSITY ★ ENERGY INSTITUTE

AB-INITIO MODELLING OF OXYGEN REDUCTION REACTION ON DOPED GRAPHENE SURFACE IN ACIDIC MEDIA

M.Sc. THESIS

Hasan Ozan AVCI
(301161018)

Energy Science and Technology Division

Energy Science and Technology Programme

Thesis Advisor: Assoc. Prof. Dr. Adem TEKİN

JULY 2019

İSTANBUL TEKNİK ÜNİVERSİTESİ ★ ENERJİ ENSTİTÜSÜ

KATKILANMIŞ GRAFEN YÜZEY ÜZERİNDEKİ OKSİJEN İNDİRGENME REAKSİYONUNUN ASİDİK ORTAMDA AB-İNİTİO MODELLENMESİ

YÜKSEK LİSANS TEZİ

Hasan Ozan AVCI
(301161018)

Enerji Bilim ve Teknoloji Anabilim Dalı

Enerji Bilim ve Teknoloji Programı

Tez Danışmanı: Doç. Dr. Adem TEKİN

TEMMUZ 2019

Hasan Ozan AVCI, a M.Sc. student of ITU Energy Institute student ID 301161018, successfully defended the thesis entitled "AB-INITIO MODELLING OF OXYGEN REDUCTION REACTION ON DOPED GRAPHENE SURFACE IN ACIDIC MEDIA", which he prepared after fulfilling the requirements specified in the associated legislations, before the jury whose signatures are below.

Thesis Advisor :	**Assoc. Prof. Adem TEKİN** Istanbul Technical University	.....
Jury Members :	**Prof. Dr. Nilgün KARATEPE YAVUZ** Istanbul Technical University	.....
	Assoc. Prof. Dr. Hikmet Hakan GÜREL Kocaeli University	.....

Date of Submission : 03 May 2019
Date of Defense : 16 July 2009

To my dear family,

FOREWORD

First of all, I would like to express my sincere appreciations to my dear thesis advisor; Assoc. Prof. Dr. Adem Tekin for guiding me through his reviews and for all his supports during the thesis.

I would like to extent my heartfelt gratitude to Mehmet Çankaya for his support during the study.

I also would like to thank dear jury members; Prof. Dr. Nilgün Karatepe Yavuz and Assoc. Prof. Dr. Hikmet Hakan Gürel for their valuable time.

Especially, I am deeply grateful to dear Bilge Can, for standing by my side during the whole process and supporting me unconditionally.

Finally, I would like to convey my sincere thankfulness to my dear family members, for their genuine belief in me throughout my life.

July 2019

Hasan Ozan AVCI
(Mechanical Engineer)

TABLE OF CONTENTS

Page

ABBREVIATIONS

AFC	**:** Alkaline Fuel Cells
BO	**:** Bohr-Oppenheimer
DFT	**:** Density Functional Theory
DMFC	**:** Direct Methanol Fuel Cells
GGA	**:** Generalized Gradient Approximation
HER	**:** Hydrogen Evolution Research
LDA	**:** Local Density Approximation
MCFC	**:** Molten Carbonate Fuel Cells
MEP	**:** Minimum Energy Path
NASA	**:** National Aeronautics and Space Administration
NEB	**:** Nudge Elastic Band
ORR	**:** Oxygen Reduction Reaction
PAFC	**:** Phosphoric Acid Fuel Cells
PEMFC	**:** Proton Exchange Membrane Fuel Cells
PES	**:** Potential Energy Surface
SOFC	**:** Solid Oxide Fuel Cells

LIST OF TABLES

Page

LIST OF FIGURES

Page

AB-INITIO MODELLING OF OXYGEN REDUCTION REACTION ON DOPED GRAPHENE SURFACE IN ACIDIC MEDIA

SUMMARY

The accumulation of scientific knowledge resulted with the process of great technological developments in the eighteenth century, which is called Industrial Revolution. Due to the speed in production of information and technological developments, human population has increased and this increase in population has brought increasing needs. The human need can be considered as an equivalent to human intervention in nature, which usually has not been nature-friendly until today. As a result of the increase in the energy demand, fossil fuels have evolved into one of the fundamental energy sources over time. However, the emission of greenhouse gases from fossil fuel use leads to the global climate change. Therefore, it is essential to develop more sustainable and ecosystem-friendly practices and technologies in all areas, especially to reduce the greenhouse gas emissions. This necessity of sustainable and climate-friendly energy technologies has become the main motivation of this thesis.

Fuel cells are one of the clean, renewable and efficient electro-chemical energy conversion systems. Usually, hydrogen is used as fuel and water & electricity is produced by its reaction with oxygen. The classification of fuel cells is dependent on the electrolyte types; the most well-known varieties are proton exchange membrane fuel cells, solid oxide fuel cells, phosphoric acid fuel cells, molten carbonate fuel cells and alkali fuel cells. Fuel cell systems, which are highly scalable for different applications, can be designed for several purposes ranging from transportation vehicles to stationary power plants. The technology of fuel cells, which dates back nearly two hundred years ago, has not been commercialized yet to the desired levels. One of the most important reasons for this situation is the noble metals used as catalysts in fuel cell electrodes.

There are two reactions which establishes the basic working principle of fuel cells. The first is hydrogen evolution reaction (HER) at the anode electrode and the second one is the oxygen reduction reaction (ORR) at the cathode electrode. ORR can occur in two different ways. While the first is called two-electron ORR in which hydrogen peroxide derivatives are formed as products in the reaction chain, the second is called four-electron ORR which has a higher reversible potential than the first one. Therefore, it is preferable that ORR occurs in this way. ORR is a reaction that cannot spontaneously occur and must be supported by a catalyst. Therefore, expensive electrode materials are used to catalyse the ORR.

In recent years, graphene-based materials have become prominent as catalysts in fuel cell. Although graphene has been discovered recently, it has become an important research topic due to its essential properties in many areas. Although the catalyst properties of pure graphene are not satisfactory, it has become considered as an important catalyst material through various strategies. Essentially, two strategies have become prominent in graphene catalyst research. While the first is the addition of different types of atom to graphene, the second is to create various surface deformations. The main purpose of both strategies is to increase the active sites on the surface to obtain high catalytic properties. In terms of first strategy, various transition metals are investigated in addition to non-metal dopants such as nitrogen, boron, sulphur, phosphorus. Additives can be both double/triple and metal/non-metal dopants can be doped on the same surface. It has been observed that different doping conditions positively affect the catalytic properties of the surface. In terms of second strategy, it is the most preferred to create vacancies on the surface to which dopants can be bonded. It has also been observed that the formation of voids on the surface, without any additive, increases the catalytic effect. ORR can occur in acidic and alkaline environments according to the operating principle of the fuel cell. There are several studies on ORR both in acidic and alkaline environments. In this study, $N_2S_2V_1$-graphene, which contains two nitrogens, two sulphurs and two vacancies in addition to transition metals (platinum, gold, silver and manganes), is selected to investigate the four-electron ORR in acidic media.

In comparison to many of other similar structures, $N_2S_2V_1$-graphene has a relatively low metal binding characteristic. In general, structures which have low formation and metal binding energies are more preferred for ORR modelling. In this study, relatively high metal binding energy structure is preferred, and its effects could be compared with other studies. In this study, the performance of metal-doped and metal-free graphene-based catalyst for ORR has been investigated and compared with other studies. The process of modelling the ORR is divided into five sub-steps which are oxygen dissociation on surface, hydrogenation of the first oxygen, removal of the first water molecule, hydrogenation of the second oxygen and finally removal of the second water molecule.

In the study, density functional theory (DFT) calculations together with path techniques (nudged elastic band (NEB)) are performed to determine reaction barriers. DFT is a quantum mechanical method which gives successful results in explaining the electronic properties of materials. The structures to be calculated must be in the ground state energy for the calculations made by DFT. In the thesis, all DFT calculations are performed with Quantum Espresso program. The structures in the initial and final cases were subjected to geometry optimization for the determination of each reaction barrier and the structures with the lowest energy are selected for the reaction barrier calculations. The reaction barrier between the resulting initial and final configurations is located by the NEB method. As a result of the determination of the reaction barriers, it becomes possible to compare the performance of the catalyst with other ones present in the literature. In non-metallic doped graphene all reaction barriers are obtained higher than the metallic doped graphene. Non-metallic doped graphene's first step barrier is 1.493 eV and the barrier values which belong to Ag, Au, Mn and Pt-doped structures, are 1.105 eV, 1.26 eV, 1.059 eV and 1.09 eV, respectively. The highest barriers are achieved in the oxygen dissociation step of ORR. The first water removal steps have lower barrier values rather than the second water molecule removal steps.

KATKILANMIŞ GRAFEN YÜZEY ÜZERİNDEKİ OKSİJEN İNDİRGENME REAKSİYONUNUN ASİDİK ORTAMDA AB-INITIO MODELLENMESİ

ÖZET

İnsanlığın bilimsel birikimi 18. yüzyılın sonlarında büyük teknolojik gelişmelerin önünü açmış ve tarihçiler tarafından Sanayi Devrimi olarak adlandırılan süreç başlamıştır. Bilginin üretim hızı ve teknolojik gelişimin artması insan nüfusunu artırmış, artan nüfus beraberinde artan ihtiyaçları getirmiştir. İnsan ihtiyacı insanın doğaya müdahalesiyle eşdeğerdir ve bu müdahale bugüne kadar çoğunlukla doğa dostu olmamıştır. Artan enerji ihtiyacını karşılamak için fosil yakıtlar zaman içinde temel enerji kaynaklarına dönüşmüştür. Fosil yakıt kullanımı kaynaklı sera gazı salınımının yarattığı sera etkisi küresel iklim değişikliğine yol açmaktadır. Bugün geldiğimiz noktada sera gazı emisyonlarını azaltmak başta olmak üzere her alanda daha sürdürülebilir ve ekosistem dostu uygulama ve teknolojileri yaygınlaştırmak zorunludur. Bu motivasyonla sürdürülebilir ve iklim dostu enerji teknolojileri son yıllarda daha da önem verilen bir araştırma alanına dönüşmüştür.

Başlıca temiz enerji teknolojilerinden birisi de yakıt hücresi sistemleridir. Yakıt hücreleri elektrokimyasal enerji dönüşüm sistemleridir. Çoğunlukla yakıt olarak hidrojen kullanılmakta ve hidrojenin oksijenle tepkimeye sokulması sonucunda elektrik ve su üretilmektedir. Yakıt hücreleri elektrolit tiplerine göre sınıflandırılırlar. En bilinen çeşitleri proton değişim membranlı yakıt hücreleri, katı oksit yakıt hücreleri, fosforik asit yakıt hücreleri, erimiş karbonat yakıt hücreleri ve alkali yakıt hücreleridir. Pek çok farklı uygulama için ölçeklenebilirliği yüksek olan yakıt hücresi sistemleri ulaşım araçlarından, sabit enerji üretim santrallerine kadar farklı amaçlar için tasarlanabilirler. Yakıt hücrelerinin diğer temiz enerji üretim sistemlerine göre emre amade enerji üretim sistemleri olmasıyla ön plana çıkmaktadır. Özellikle ulaşım kaynaklı karbon emisyonlarının azaltılması konusunda gelecekte önemli bir alternatif olmaya adaydır.

Yakıt hücrelerinde performansı etkileyen dört temel parametre vardır. İlki tersinir termodinamik gerilim değeri, geriye kalan üç tanesi ise kayıplardır. Performansı düşüren üç tane kayıp mekanizması vardır. Bunlardan ilki aktivasyon kayıpları, ikincisi ohmik kayıplar sonuncusu ise konsantrasyon kayıplarıdır. Ohmik kayıplar yük taşınımı ile ilgili olup yakıt hücresinin dış devresinde elektronların hareket etmesi sonucu ve elektrotlarda oluşan iyonların elektrolit boyunca taşınması sonucu oluşur. Konsantrasyon kayıpları, elektrotlara yakıtın ve oksidantın beslenmesi ile ilgilidir. Yakıt hücrelerinde performansa etki eden son kayıp olan aktivasyon kayıpları ise yakıt hücresinin temel çalışma prensibini oluşturan elektrot reaksiyonlarının kolaylıkla gerçekleşebilmesiyle ilgilidir. Aktivasyon kayıpları anot ve katot elektrotta görülmektedir. Tepkimelerin aktivasyon bariyerlerinin yüksek olması aktivasyon kayıplarını artırmakta ve performans kaybına yol açmaktadır.

Yakıt hücrelerinin temel çalışma prensibini oluşturan iki reaksiyon vardır. Bunlardan birincisi anot elektrotta gerçekleşen hidrojen oluşma reaksiyonu (HOR), diğeri ise katot elektrotta gerçekleşen oksijen indirgenme reaksiyonudur (OİR). OİR iki farklı yol izleyerek gerçekleşebilir. Birincisi iki elektronlu reaksiyon olarak adlandırılır ve hidrojen peroksit ürün olarak reaksiyon zinciri içerisinde oluşur. İkinci yol ise dört elektronlu OİR olarak adlandırılır ve ilkine göre tersinir potansiyeli daha yüksek olduğundan OİR'in bu yolla gerçekleşmesi daha çok tercih edilir. OİR doğası gereği kendiliğinden gerçekleşemeyen ve katalizörle desteklenmesi gereken bir reaksiyondur. Pahalı elektrot malzemeleri OİR reaksiyonunu kataliz etmek için kullanılır.

Tarihi yaklaşık 200 yıl öncesine dayanan yakıt hücresi teknolojisi hala istenen seviyelerde ticarileşememiştir. Bu durumu yaratan en önemli sebeplerden ilki yakıt olarak kullanılan hidrojenin depolanmasındaki güçlükler ikincisi ise yakıt hücresi elektrotlarında aktivasyon kayıplarını azaltmak için katalizör olarak kullanılan pahalı malzemelerdir. ikinci Platin gibi soy metallerin performans kaybını minimize etmek için yoğun olarak kullanılması yakıt hücresi sistemlerinin birim maliyetlerini yükseltmekte ve bu durum yakıt hücresi sistemlerinin enerji pazarındaki rekabet gücünü azaltmaktadır. Bu çalışmada yakıt hücresi sistemleri için alternatif katalizör malzemelerinin özellikleri araştırılmış olup, yakıt hücresi teknolojisinin yaygınlaşmasının önündeki önemli engellerden bir tanesinin aşılabilmesine katkı sağlayabilmek hedeflenmiştir.

Son yıllarda yakıt hücrelerinde katalizör olarak kullanılmak üzere grafen temelli malzemeler öne çıkmaktadır. Grafen yakın geçmişte bulunmuş olmasına karşın birçok alandaki iyi özellikleri onu önemli bir araştırma konusu haline getirmiştir. Saf grafenin katalizör özellikleri tatmin edici olmasa da çeşitli stratejilerle önemli bir katalizör malzemesi olabileceği görülmüştür. Temel olarak iki strateji grafen katalizör araştırmalarında öne çıkmıştır. Bunlardan ilki grafeni farklı atom türleriyle katkılamak ikincisi ise çeşitli yüzey deformasyonları yaratmaktır. Her iki stratejinin de temel amacı yüzey üzerindeki aktif bölgeleri artırarak yüksek kataliz özelliği elde etmektir. İlk strateji bağlamında azot, bor, sülfür, fosfor gibi metal olmayan katkılayıcılara ek olarak çeşitli geçiş metalleri de katkılayıcı olarak araştırılmıştır. Katkılamalar ikili, üçlü olabildiği gibi metal ve metal olmayan katkılayıcılar da aynı yüzey üzerine katkılanabilmektedir. Farklı katkılama durumlarının yüzeyin katalitik özelliklerini olumlu etkilediği görülmüştür. İkinci strateji bağlamında ise yüzey üzerinde katkılayıcıların bağlanabileceği alanlar yaratmak en çok tercih edilen yoldur. Herhangi bir katkılayıcı olmadan da yüzey üzerinde boşluklar oluşturmanın katalitik etkiyi artırdığı gözlenmiştir. OİR yakıt hücresinin çalışma prensibine göre asidik ya da alkali ortamda gerçekleşebilir. Ortamın asidik ya da alkali olması temel yakıt hücresi reaksiyonlarında farklılık yaratır. Literatürde hem asidik ortamda hem de alkali ortamda gerçekleşen OİR için çalışmalar mevcuttur. Bu çalışmada OİR asidik ortamda modellenmiştir.

Deneysel ve teorik çalışmalar azot ve sülfürün beraber katkılanmış oldukları grafen yapıların sadece azot katkılanmış yapılardan daha iyi katalitik özelliklere sahip olduğunu göstermiştir. Bu sebeple, bu çalışmada iki azot ve iki sülfür atomu ile katkılanmış bir boşluklu grafen ($N_2S_2V_1$-grafen) yüzey esas alınmış; metalsiz yapı ve çeşitli metallerin (platin, altın, gümüş ve manganez) ayrı ayrı katkılandığı toplamda beş farklı yapı üzerinde asidik ortamda dört elektron reaksiyon mekanizmasına sahip OİR modellenmiştir. $N_2S_2V_1$-grafen, yapının formasyon enerjisi ve metal bağlama enerjisine göre seçilmiştir. Seçilen yapının metal bağlama enerjisi daha önce bilgisayar

ortamında modellenen olası yapılara göre bir miktar yüksektir. Genel olarak düşük formasyon enerjisine ve metal bağlama enerjisine sahip yapılar OİR modellemesi için daha çok tercih edilir. Bu çalışmada görece yüksek metal bağlama enerjili yapı tercih edilerek bu durumun etkileri de literatürle kıyaslanabilmiştir. Bu çalışmada metal katkısız veya metal katkılı grafenin OİR için performansı değerlendirilmiş ve literatürle kıyaslanmıştır.

OİR modellenirken kendi içinde beş alt basamağa ayrılmış ve bu basamaklardaki reaksiyon bariyerleri hesaplanmıştır. Bu basamaklardan ilki yüzeye tutunan oksijenin ayrışması, ikincisi ayrışan oksijenlerden ilkinin yüzeyden hidrojen alması, üçüncüsü yüzey üzerinde oluşan hidroksit grubunun yüzey üzerinden bir hidrojen daha alarak ilk su molekülünün uzaklaştırılması, dördüncüsü yapı üzerine bağlı ikinci oksijenin yüzeyden hidrojen alması ve son adım yapı üzerine bağlı hidroksit grubunun yapıdan bir hidrojen daha alarak ikinci su molekülünün uzaklaşmasıdır. Beş adım sonunda dört mol hidrojen iyonu, bir mol oksijen molekülü ve dört elektron tüketilerek iki mol su molekülü oluşturulmuştur.

Bu çalışmada reaksiyon bariyerlerinin belirlenebilmesi için yoğunluk fonksiyonel teorisi (YFT) ve minimum enerji yolu bulma tekniği (dürtülü elastik bant (DEB)) birlikte kullanılmıştır. YFT malzemelerin elektronik özelliklerini açıklamakta başarılı sonuçlar veren bir kuantum mekanik yöntemdir. YFT kullanılarak yapılacak hesaplamalarda, hesaplanacak yapıların taban durum enerjisinde bulunması zorunludur. Bu çalışmada tüm YFT hesaplamaları Quantum Espresso programıyla yapılmıştır. Belirlenecek her reaksiyon bariyeri için başlangıç ve son durumlardaki yapılar geometri optimizasyonuna tabi tutulup en düşük enerjili yapılar reaksiyon hesapları için seçilmiştir. Belirlenen başlangıç ve final konfigürasyonları arasındaki reaksiyon bariyeri DEB metoduyla belirlenmiştir. Belirlenen reaksiyon bariyerleri sonucunda incelenen yapıların kendi içinde ve literatürdeki örneklerle karşılaştırılabilmesi imkânı doğmuştur.

Tez çalışması süresince beş yapı üzerindeki bütün reaksiyon adımlarının bariyerlerinin belirlenmesi tamamlanamamış fakat elde edilen sonuçlar tez için yeterli görülmüştür. Devam eden süreçte eksikler tamamlanacak ve yeni metal katkılayıcılar için de hesaplamalar yapılacaktır. Altın katkılanmış yapı üzerinde tüm reaksiyon adımlarının bariyerleri belirlenmiş, platin, gümüş ve metal katkılanmamış yapılar için dört reaksiyon adımının reaksiyon bariyerleri belirlenmiş, manganez katkılanmış yapı için iki reaksiyon adımının reaksiyon bariyerleri belirlenebilmiştir. İlk reaksiyon adımı modellenirken yüzey üzerindeki birkaç olası aktif bölgenin üzerine oksijen molekülü yerleştirilmiş ve bunlar arasından en düşük enerji değerine sahip optimize yapı hesaplamaların başlangıcı için seçilmiştir.

Şimdiye kadar elde edilen sonuçlara göre literatürle benzer olarak metal katkılamanın azot ve sülfür katkılanmış yapıda katalitik etkiyi artırdığı ve tüm reaksiyon adımlarında reaksiyon bariyerini düşürdüğü görülmüştür. Bu bağlamda ilk reaksiyon adımının bariyer değerleri metalsiz, gümüş katkılanmış, altın katkılanmış, manganez katkılanmış ve platin katkılanmış yapılar için sırasıyla 1.493 eV, 1.105 eV, 1.26 eV, 1.059 eV ve 1.09 eV olarak bulunmuştur. Alınan sonuçlara göre en yüksek enerji bariyerli reaksiyon adımı oksijen ayrılma adımı (ilk adım) olduğu görülmüştür. Öte yandan, prosesleri aynı olmasına rağmen ikinci ve üçüncü adımlarda oluşan reaksiyon bariyerlerinin dördüncü ve beşinci adımlarda oluşan reaksiyon bariyerlerine göre daha düşük olduğu görülmüştür.

1. INTRODUCTION

Energy demand of the world has been increasing day by day since the Industrial Revolution. As a result of exponential population growth, the impact of humanity on natural balance is increasing. However, natural resources have been consumed at the highest level in the history of the world and environmental destruction reached an excessive amount in today. The most well-known consequence of this destructive behaviour of humanity on nature is the climate change.

Due to this increase of energy demand, fossil fuel resources became the primary energy source. However, usage of fossil fuels became an unsustainable activity in the near past. The amount of greenhouse gasses in the atmosphere reached to a crucial level due to the combustion chemistry of carbon-based resources. Therefore, the renewable, clean and efficient energy production technologies came forward in the last decades.

One of these renewable, clean and efficient energy technologies is fuel cell technology. A fuel cell is an electrochemical energy conversion device which converts chemical energy into electrical energy directly. It produces energy by reacting hydrogen and oxygen. Fuel cells are very scalable systems which can be used from small transportation application like automobiles or trucks to stationary power plants at MW scale.

Some of the well-known types of fuel cells are proton exchange membrane fuel cells (PEMFC), alkaline fuel cells (AFC), molten carbonate fuel cells (MCFC), phosphoric acid fuel cells (PAFC), direct methanol fuel cells (DMFC) and solid oxide fuel cells (SOFC). There are four parameters which affects the fuel cell performance. These are ideal reversible thermodynamic output, activation losses, ohmic losses and concentration losses. Activation losses which are caused by electrode reactions, are highly dependent on activation barriers of fuel cell electrode reactions and significantly affects the fuel cell performance. Therefore, fuel cells require expensive catalyst like platinum must be replaced with abundant and cheaper alternatives in order

to minimize activation losses, especially at the cathode part of fuel cell, where oxygen reduction reaction (ORR) occurs.

Fuel cell technology dates back to nearly two hundred years. However, from its invention to today's commercialized fuel cell technology, it still could not reach to a satisfactory level. There are two main reasons behind this fact. One of these is hydrogen storage for portable fuel cell applications and the second one is expensive electrode materials which increase the unit price of a fuel system. For instance, in a PEM fuel cell stack the electrode part is half of the cost [1]. In order to increase the competitiveness of fuel cell technology, effective and cheaper electrode materials play a vital role.

Since from its invention in 2004 [2], graphene has attracted researchers' attention with its extraordinary properties. However, catalytic property of intrinsic graphene is not good enough for ORR [3]. Because of this reason, some strategies have been developed for enhancing catalytic activity of graphene. These strategies can be summarized in two main categories. The first strategy is hetero-atom doping and the second strategy is the creation of defects on graphene surface. Both strategies aim to increase active sites of surface, thereby, improving the catalytic activity.

Under the first strategy nitrogen, boron, sulphur and phosphor doping are studied extensively [4-9]. ORR performance of nitrogen doped graphene is comparable with platinum-based catalyst [10]. Moreover, other non-metallic dopant species show better catalytic activity than undoped graphene [11]. In addition to non-metallic dopants, metallic dopants also have a positive effect on the ORR activity. Precious and non-precious metal doping variations were reported in the literature [12-15]. With the combination of non-metallic dopant species such as N-S, N-B, N-P, dual-doped effects were also investigated in the previous studies. Even N-S-P triple doping was studied [16,17]. Metallic and non-metallic dual doping strategy was also investigated [18-20]. Creating vacancies on a surface is the second strategy for improving the catalytic activity of graphene-based materials. Defects on the surface become active sites for electrocatalytic reactions, hence, the ORR activity increases [21,22].

Oxygen dissociation step of ORR requires more activation barrier relatively compared to the other steps of reaction. Some DFT based studies showed that different type of hetero-atom doped graphene surfaces give different results on especially oxygen

dissociation step of ORR. The study of Zheng et.al [23] determines the reaction barrier of oxygen dissociation step of ORR in pure, N-doped and transition metal graphene. For pure graphene, three different pathways of oxygen dissociation were investigated and reaction barriers were determined to be 2.71 eV, 3.73 eV and 3.35 eV, respectively. Two different oxygen dissociation pathways were investigated on N-doped graphene and the following reaction barriers were calculated: 1.85 eV and 1.70 eV, respectively. Finally, oxygen dissociation barriers were calculated to be 1.14 eV, 1.16 eV, 0.95 eV and 1.45eV, respectively on Fe, Co, Ni and Cu doped graphene. Another study which conducted by Yang. et.al. [24] compares oxygen dissociation barriers of different transition metal and nitrogen doped graphene surface, which has four nitrogens and two vacancies. Reaction barriers were calculated to be 1.03 eV, 0.61 eV, 1.22 eV, 0.90 eV and 1.45 eV for Ti, V, Cr, Mn and Fe doped N-graphene surface respectively. As it can be deduced from these studies, different kind of strategies differs the ORR activity.

In this study, $N_2S_2V_1$-graphene, which contains two nitrogens, two sulphurs and two vacancies in addition to transition metals, is selected to investigate the ORR activity. In comparison to many of other similar structures which are designed by Mehmet Çankaya for his PhD thesis, $N_2S_2V_1$-graphene has a relatively high metal binding energy. In some fuel cell types like PEMFCs and PAFCs, ORR reaction occurs in acidic media. Also, in this study, ORR is modelled in acidic media. ORR can occur in two pathways. The first possible pathway is a two-electron pathway and the second one is a four-electron pathway. Equation 1.1 and 1.2 represent two and four electron pathways.

$$H_2 + \frac{1}{2}O_2 + 4e^- \rightarrow H_2O \quad (1.1)$$

$$H_2 + O_2 + 2e^- \rightarrow H_2O_2 \quad (1.2)$$

For this study, four-electron pathway is selected since it is more favourable for electrochemical energy conversion devices. Selected pathway contains five sub-steps which are oxygen dissociation on surface, hydrogenation of the first oxygen, removal of the first water molecule, hydrogenation of the second oxygen and finally removal of the second water molecule. All of these sub-steps were modelled on $N_2S_2V_1$-

graphene, Ag-$N_2S_2V_1$-graphene, Au-$N_2S_2V_1$-graphene, Mn-$N_2S_2V_1$-graphene and Pt-$N_2S_2V_1$-graphene.

Catalytic capability of selected structures is examined with computational methods. In particular, periodic DFT calculations were employed and subsequent nudged elastic band (NEB) calculations were performed to study the reaction barriers.

2. FUEL CELL

In the scope of this chapter, firstly, history of fuel cell technology is explained. Afterwards, working principle, main components and types of the technology are introduced. At the end of the chapter, ORR deeply discussed, and more details are given about the role of ORR in fuel cell technology.

2.1 Fuel Cell History

During nineteenth century, electrochemistry was a hot research area. Although some of the main concepts of electrochemistry had been discovered, there were still undiscovered ones yet. The simple idea of generating electricity by reverse electrolysis process was studied by William R. Grove. Within this simple framework, Grove started his experiments. First fuel cell was consisted of dilute sulfuric acid as electrolyte, two porous platinum rods as electrodes and hydrogen and oxygen gases as reactants. He published his first paper on this experiment in 1839 [25] Figure 2.1 contains schematic demonstration of Grove's fuel cell.

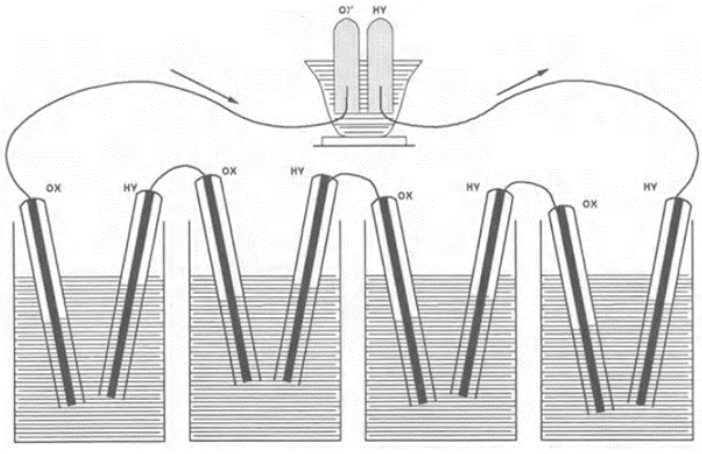

Figure 2.1 : Groove's fuel cell [25].

After his invention, some researches were conducted by several scientists, however, expensive platinum electrode and low rated power values were slowed down the fuel cell research [26]. Francis Thomas Bacon was started working on fuel cells for developing a fuel cell which does not have platinum electrodes and generates more

electricity. In 1939, Bacon built his first single cell which operated with nickel electrodes and KOH electrolyte. His first cell operated under the conditions of 200 °C temperature and 220 bar pressure, it was also the first fully operating fuel cell in the history of electricity generation. Bacon improved the operating conditions and power output of his fuel cell in the following years [26].

In the early 1950s, more importance on fuel cell technology was given by NASA. Energy supply in spacecrafts for long time missions was a challenge at that years. Battery technology was not capable enough and NASA needed a system which has more power density. Therefore, NASA developed an alkaline fuel cell based on Bacon's design for Apollo space program and it was used in spacecrafts [27].

Afterwards, General Electric built first solid polymer membrane fuel cell system which had 1 kW power output for Gemini space program as power supplier of spacecrafts. This system was used in seven spacecrafts in Gemini program [28]. Figure 2.2 contains photographs of the fuel cells which are used in the space programs.

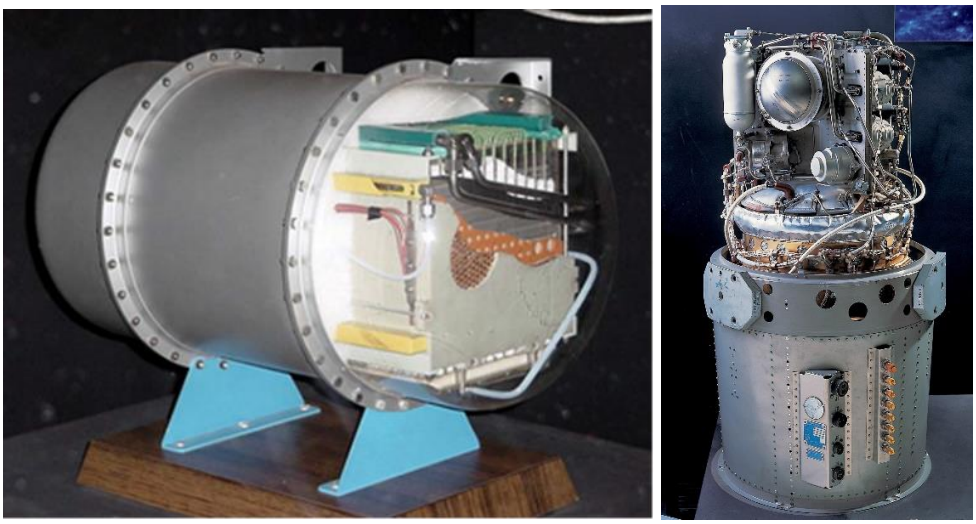

Figure 2.2 : Fuel cells used in Gemini (left) and Apollo space programs [29-30].

A patent citation-based study [31], which was conducted for mapping the historical trajectory of fuel cell technology showed that the most exponential growth of fuel cell-based patent citations observed in the period between 1950s and 1970s. Although this increasing trend of patent citations is continuing, the speed of growth is slower today with respect to the stated period.

Another study on the historical development of fuel cell technology [32], which is focused on directly patent numbers on fuel cell topic, followed similar pathways. In

that study, fuel cell history divided in three parts. Between the years of 1873 and 1958, the first part is named as emerging phase, which contains developments of main concepts on fuel cell technology. The second part, which is dated between 1959 and 1990, is named as growth phase. In this phase, fuel cell research was boomed, and fuel cells appeared as an alternative energy supplier either for critical missions like space programs or for the commercial market. The third and the last between 1990 and 2002 is named as diffusion phase. In this phase fuel cell patents showed an exponential growth. After the second part of fuel cell history, the technology was proved itself. From the beginning of the third part of its history to present, fuel cell research motivated by developing more efficient, more durable and more cost-effective systems for replacing traditional energy production systems with a more environmentally friendly choice.

2.2 Main Aspects of Fuel Cells

A fuel cell is an electrochemical energy conversion device. Its conversion process can be explained by a reaction which is sum of two different reactions.

$$H_2 \rightarrow 2H^+ + 2e^- \tag{2.1}$$

$$\frac{1}{2}O_2 + 2H^+ + 2e^- \rightarrow H_2O \tag{2.2}$$

The first reaction (2.1) is called as hydrogen evolution reaction (HER) and the second one is the oxygen reduction reaction (ORR). The basic operation of a single fuel cell includes the following steps;

- As a fuel commonly hydrogen, separated hydrogen ions at anode electrode,
- After HER, freed electrons are collected by external circuit and hydrogen ions are carried by electrolyte to cathode electrode,
- At the cathode part of cell oxygen reduces to water taking electrons from external circuit and hydrogen ions from electrolyte.
- At the end of one cycle single fuel cell consumes two hydrogen molecules and one oxygen molecule and generates electricity and water.

A schematic representation about the basic fuel cell operation is given in Figure 2.3.

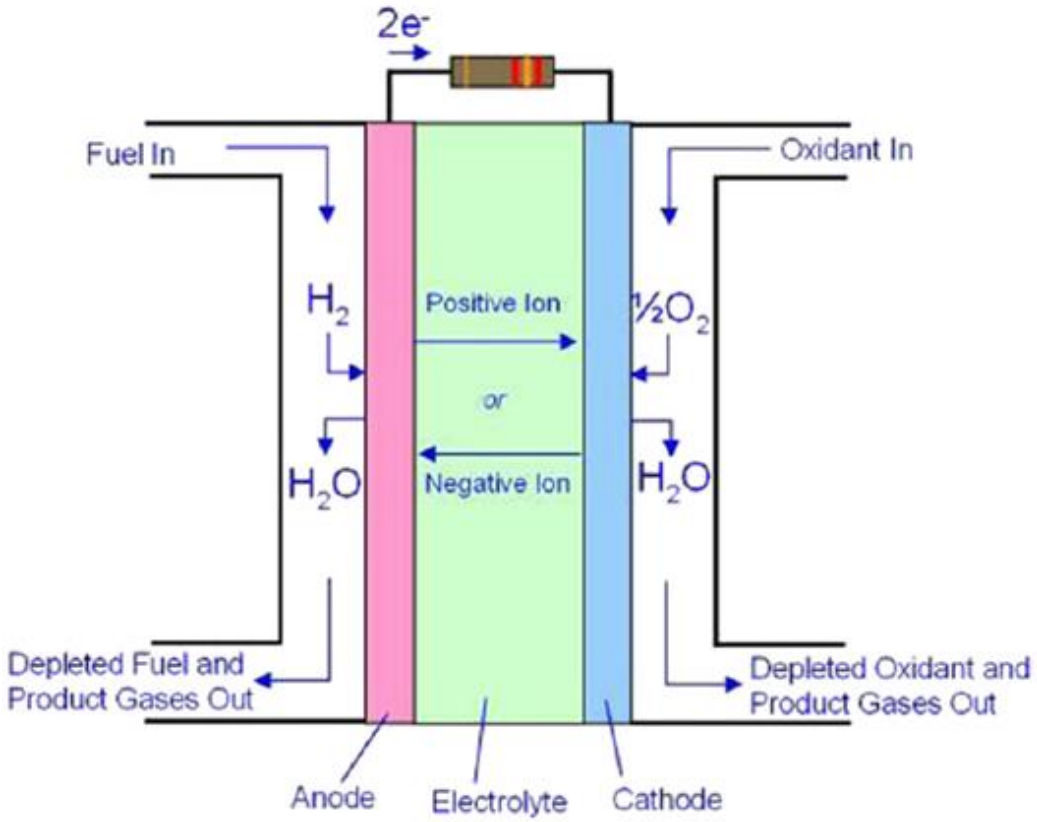

Figure 2.3 : Basic operation of fuel cells [33].

The main components of fuel cells are gas diffusion layers, anode and cathode electrodes and electrolyte. Fuel cells generally classifies according to their electrolyte type. Six types of fuel cells come forward which are PEMFC or PEFC, AFC, DMFC, PAFC, MCFC SOFC. A comparison for different types of fuel cells is given in Table 2.1.

In order to determine a single fuel cell's performance firstly ideal maximum output should be calculated. When the total reaction considered as fully reversible and losses is neglected, the total voltage output of reaction is given in Table 2.2.

Table 2.1 : Comparison of fuel cell types [34].

Fuel cell type	Electrolyte	Operating temperature	Charge carrier ion	Anode Reactions	Cathode Reactions
PEMFC	Polymer membrane	60-140 ℃	H^+	$H_2 \rightarrow 2H^+ + 2e^-$	$\frac{1}{2}O_2 + 2H^+ + 2e^- \rightarrow H_2O$
AFC	Potassium hydroxide	30-80 ℃	OH^-	$H_2 + 2OH^- \rightarrow H_2O + 2e^-$	$\frac{1}{2}O_2 + H_2O + 2e^- \rightarrow 2OH^-$
DMFC	Polymer membrane	150-200 ℃	H^+	$CH_3OH + H_2O \rightarrow CO_2 + 6H^+ + 6e^-$	$\frac{3}{2}O_2 + 6H^+ + 6e^- \rightarrow 3H_2O$
PAFC	Phosphoric acid	180-200℃	H^+	$H_2 \rightarrow 2H^+ + 2e^-$	$\frac{1}{2}O_2 + 2H^+ + 2e^- \rightarrow H_2O$
MCFC	Lithium/Potassium Carbonate	650 ℃	CO_3^{2-}	$H_2 + CO_3^{2-} \rightarrow H_2O + CO_2 + 2e^-$	$\frac{1}{2}O_2 + CO_2 + 2e^- \rightarrow CO_3^{2-}$
SOFC	Yittria Stabilized Zirconia	1000 ℃	O^{2-}	$H_2 + O^{2-} \rightarrow H_2O + 2e^-$	$\frac{1}{2}O_2 + 2e^- \rightarrow O^{2-}$

Table 2.2 : Reversible reactions voltages.

Reaction type	Equation	Voltage
HER	$H_2 \rightarrow 2H^+ + 2e^-$	-0.000 V
ORR	$\frac{1}{2}O_2 + 2H^+ + 2e^- \rightarrow H_2O$	+1.229 V
Total Reaction	$\frac{1}{2}O_2 + H_2 \rightarrow H_2O$	+1.229 V

The theoretical maximum voltage output of a single fuel cell is 1.229 V. Any real application cannot pass this theoretical limit because of irreversibility in the total reaction. In real case, voltage output calculated by formula given below;

$$V = E_{thermo} - \eta_{act} - \eta_{ohmic} - \eta_{conc} \tag{2.3}$$

Performance of a single fuel cell is related with four parameters in general. The first parameter is the thermo-dynamical capability of the total fuel cell reactions. This term refers to maximum possible voltage output of a single cell. The last three terms are loss terms. The first loss in a fuel cell is the 'activation loss' which occurs in both electrodes and this is directly related with catalyst process in electrodes. The second loss is the 'ohmic loss' which is related to charge transfer and occurs in both electrolyte and external circuit of fuel cell. The last loss is 'concentration loses'. This type of loss is related with oxidant and reactant concentration at electrodes. In Figure 2.4, relation between fuel cell performance and losses is given with a typical fuel cell I-V curve.

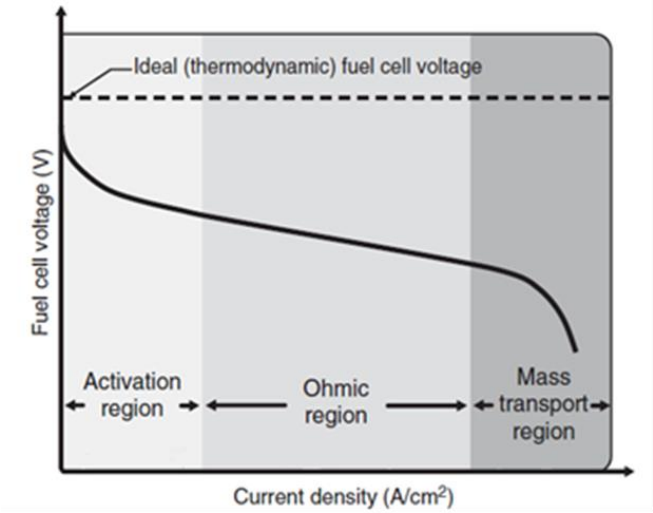

Figure 2.4 : Typical I-V curve of a fuel cell [35].

Due to the scope of this study, only activation losses are examined in detail. Activation losses can be explained as a consumption of a part of voltage generated by cell in order to pass reaction barriers and start to generate current by cell. It is related with reaction kinetics of cell. Firstly, activation energy affects probability of finding the reactant on activated states of electrodes. This relation is given in Equation 2.4.

$$P_{act} = e^{-\Delta G/(RT)} \tag{2.4}$$

In Equation 2.4, P denotes probability, ΔG denotes activation barrier, R denotes gas constant and T denotes temperature. After this statistical approach, reaction rate can be calculated by Equation 2.5.

$$I = c_R \times f_1 \times P_{act} \tag{2.5}$$

In Equation 2.5, c_R refers to reactant concentration at reaction area, f refers to decay rate and I refers to reaction rate. Decay rate can be calculated by 2.6 equation, which is given below.

$$f = \frac{kT}{h} \tag{2.6}$$

In Equation 2.6, h denotes Planck's constant, k denotes Boltzmann's constant and T denotes temperature.

Reaction rates of electrode at forward and reverse direction can be calculated by given above equations, separately. The net reaction rate of total cell can be determined also in this way. However, current density term is more proper for evaluating the performance of a fuel cell. After the calculation of reaction rates, current densities can also be calculated. The relation between reaction rate and current density is given by Equation 2.7.

$$i = n \times F \times I \tag{2.7}$$

In Equation 2.7, n refers to the number of electrons which are produced at the end of the reaction and F denotes to Faraday's constant. After this contribution, current density formula can be expressed with Equation 2.8.

$$i = n \times F \times c_R \times f \times e^{-\Delta G/(RT)} \tag{2.8}$$

Exchange current density is a term defined as reaction rate at equilibrium state. At equilibrium state both anode and cathode reaction rates must be equal and exchange current density, i_0, can be calculated by equation 2.9.

$$i_1 = i_2 = i_0 \tag{2.9}$$

In practice, fuel cell operation mostly goes on at non-equilibrium state. When a system went away from equilibrium state, current density is calculated by the following Buttler-Volmer Equations.

$$i_1 = i_0 \exp(\alpha nF\eta / (RT)) \tag{2.10}$$

$$i_2 = i_0 \exp[-(1-\alpha)nF\eta / (RT)] \tag{2.11}$$

$$i = i_0[\exp(\alpha nF\eta / (RT)) - \exp(-(1-\alpha)nF\eta / (RT)) \tag{2.12}$$

The first equation is for forward reaction, the second one is for reverse reaction and the third one states net current density of a reaction. α term is related with symmetry of activation barriers of forward and reverse directions of reaction. N is the number of electrons, which are generated by reaction, F is Faraday's constant, η is the activation loss, R is gas constant and T is temperature. Butler-Volmer Equation explains how the current density is affected by activation overvoltage or in other words activation loss. Basically, it means, if current density is higher, activation loss will be higher. Tafel equation comes with an assumption to Buttler-Volmer equation for simplifying it. It states that, if η_{act} is high enough, the second exponential term of Buttler-Volmer equation can be neglected. After this assumption, Buttler-Volmer equation is reduced to the following form called as Tafel equation.

$$\eta_{act} = -\frac{RT}{\alpha nF}\ln i_0 + \frac{RT}{\alpha nF}\ln i \tag{2.13}$$

To sum up, activation energy dominantly determines the reaction rate of both anode and cathode reactions, reaction rate determines exchange current density and exchange current density determines current density and activation loss amount of a single fuel cell. Thus, voltage and current output, two parameters that determine net power output of a fuel cell, highly depends on activation barriers of reactions. This is one of the most important challenge to achieve an improved fuel cell performance and therefore it requires designing novel catalyst materials lowering activation barriers.

2.3 Oxygen Reduction Reaction

ORR is one of the fundamental reactions of electro-chemistry. It has a vital role for especially fuel cells. Many of fuel cells include ORR in the cathode part. It has two different pathways, which are classified by the amount of the consumed electrons. One of the possible pathways is two electrons ORR and the another one is four electrons ORR. ORR can occur both acidic and alkaline media. According to the reaction media, ORR reaction balances differ. In Table 2.3, ORR pathways are given.

Table 2.3 : Possible pathways for ORR in different medias.

Pathways	Acidic Media	Alkaline Media
2 electrons	$O_2 + 2H^+ + 2e^- \rightarrow H_2O_2$	$O_2 + H_2O + 2e^- \rightarrow HO_2^- + OH^-$
4 electrons	$O_2 + 4H^+ + 4e^- \rightarrow 2H_2O$	$O_2 + 2H_2O + 4e^- \rightarrow 4OH^-$

In table 2.4 sub-steps of 4 electrons ORR in acidic media is given. This pathway is followed for ORR calculations in this study.

Table 2.4 : Sub-steps of four-electrons ORR in acidic media.

Sub-steps	Reactions
First step	$O_2 + * \rightarrow O^* + O^*$
Second step	$O^* + O^* + H^+ + e^- \rightarrow OH^* + O^*$
Third step	$OH^* + O^* + H^+ + e^- \rightarrow H_2O + O^*$
Fourth step	$O^* + H^+ + e^- \rightarrow OH^*$
Fifth step	$OH^* + H^+ + e^- \rightarrow H_2O + *$

Because of the influence of activation barriers on fuel cell performance, reducing reaction barriers is a critical issue on fuel cell research. Designing an effective catalyst process is a compulsory item in ORR based electrochemical energy conversion devices due to the partite and slow nature of ORR. For this reason, many materials investigated to determine their catalytic properties. Figure 2.5 is a volcano plot of some metallic materials in activity with Sabatier's principle is plotted against to oxygen binding energies.

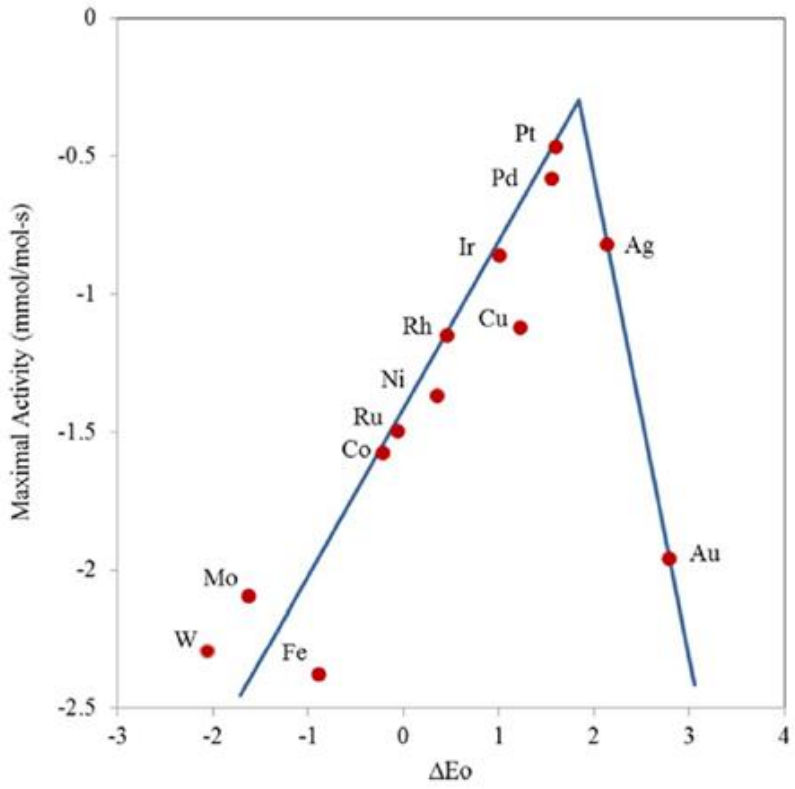

Figure 2.5 : Volcano plot of activity and oxygen binding energy relation [36].

Sabatier's principle states that a catalyst material should be able to bind the reactants strong enough to catalyse them and weak enough to dissociate to products [35]. In Figure 2.5, platinum shows the best catalytic property compared with the rest of metals; however, emptiness of peak area of plot says that there could be better catalyst materials rather than platinum.

In the recent years, graphene-based materials came forward as a promising electrocatalyst material. Graphene can be defined as 2-dimensional hexagonal configured carbon sheet. Since its invention in 2004, extensive research efforts figured out its outstanding properties. In Table 2.5 some properties of graphene are given.

Table 2.5 : Some properties of graphene [34].

Property	Value	Unit
Fracture strength	124	GPa
Density	>1	g/cm^3
Specific surface area	2630	m^2/g
Thermal conductivity	~5000	W/mK
Electrical conductivity	10^6	S/cm
Charge mobility	200,000	cm^2/Vs

Besides significant properties of intrinsic graphene, its ORR activity is not favourable. Due to this reason various strategies are developed to improve its electro-catalytic properties for ORR. For increasing active sites on the graphene-based surface, one of the most favourable strategy is hetero-atom doping on graphene surface. Nitrogen, boron, sulphur, precious or non-precious metals positively contribute to the catalytic property of graphene. In addition, dual doping strategies is favourable too. Beyond doping, creating vacancies on surface is also increases active sites and ORR activity. In this study, a N-S and metal doped graphene surface with a vacancy is investigated to determine its catalytic properties of ORR.

3. METHODOLOGY

In this chapter, methodological aspects of the study will be discussed. Firstly, the foundations of methodology, Schrödinger equation and density functional theory will be summarized. Afterwards, the nudged elastic band method, which is used for finding minimum energy paths of reactions will be explained.

3.1 Schrödinger Equation

While classical mechanics are more suitable to study nano-scale and beyond systems, quantum mechanics is used to describe much smaller systems containing up to 100 atoms in a reasonable accuracy. The first quantum mechanics concepts arose at the early twentieth century. Erwin Schrödinger, who was an Austrian scientist, in 1926 published his equation which is called by his name. In chemistry, mostly time-independent form of this equation is used. The time independent Schrödinger equation is given by Equation 3.1.

$$\hat{H}\Psi = E\Psi \tag{3.1}$$

In Equation 3.1, Ψ represents a wave function, E represents energy and $\hat{H}$ represents Hamiltonian of system. Detailed form of Hamiltonian operator is given in equation 3.2.

$$\hat{H} = -\frac{\hbar^2}{2m}\sum_i \nabla_i^2 - \sum_A \frac{\hbar^2}{2M_A}\nabla_A^2 - \sum_{A,i}\frac{Z_A e^2}{4\pi\varepsilon_0 r_{Ai}} + \sum_{i>j}\frac{e^2}{4\pi\varepsilon_0 r_{ij}} + \sum_{A>B}\frac{Z_A Z_B e^2}{4\pi\varepsilon_0 R_{AB}} \tag{3.2}$$

The first and second term of this equation define kinetic energies of electrons and nuclei, respectively. The rest of the terms define interactions between electrons and nuclei, interelectronic and inter-nucleic, respectively. Wave function has 3N dimensions and N represents the amount of the electrons. Because of that, solution of Schrödinger equation becomes harder and harder when the number of electrons increase in the considered system. Therefore, some approaches have been developed for solving Schrödinger equation. One of them is Bohr-Oppenheimer (BO) approximation. BO approximation suggests that, due to meaningful difference

between nuclei and electrons motion, nuclei can be considered as fixed respect to electrons. After that assumption, Schrödinger equation and total term of Hamiltonian is given in equation 3.3 and 3.4, respectively.

$$(\hat{H}_{el} + V_N)\Psi_{el} = E_{el}\Psi_{el} \tag{3.3}$$

$$\hat{H}_{el} = -\sum_i \frac{\hbar}{2m_e}\nabla_i^2 - \sum_i \sum_k \frac{e^2 Z_k}{r_{ik}} + \sum_{i<j} \frac{e^2}{r_{ij}} \tag{3.4}$$

In Equation 3.3, $\hat{H}_{el}$ represents electronic Hamiltonian, V_N denotes nuclear-nuclear Columbic energy and E_{el} is electronic energy. After BO approximation Schrödinger equation's solution becomes easier. For solving Schrödinger equation three main group of methods can be used in practice. These are ab-initio methods, semi-empirical methods and DFT. The main difference between semi-empirical methods and others is that semi-empirical methods use experimental data in calculations. Ab-initio methods use Hartree-Fock (HF) and post-HF calculations for solution on the other hand density functional methods use Hohenberg-Kohn theorems and Kohn-Sham equations. In this study periodic DFT method is used for all calculations.

3.2 Density Functional Theory

DFT is a successful quantum mechanical approach for computing electronic properties of many body systems by using the electron density at the ground state. The theory simplifies the Schrödinger's equation with considering electron density of a system at the ground state. Its simplification is significant because wave function of a system has 3-N dimensions where N is the number electrons of system but DFT reduces it to only spatial three dimensions.

First, Thomas-Fermi suggested the concept of using electron density for explaining any system's properties in 1927. However, its insufficient solutions on complex molecular systems led to the development of today's DFT. In 1964, Hohenberg and Kohn formed DFT with two theorems [37]. The first theorem proves that ground state electron density functional in the spatial coordinates determines properties of ground state energy and wave function. The second one defines a property of energy functional, which is mentioned in the first theorem for solving Schrödinger's equation. The second theorem demonstrates that the ground state density, which minimizes the

universal energy functional, is the exact ground state density, which comes from Schrödinger equation's solution. In 1965, Kohn-Sham equations formulated for solving Hohenberg-Kohn theorem's outcomes [38]. Kohn-Sham equations given below in equation 3.5.

$$E[\rho] = T_s[\rho] + J[\rho] + \int \upsilon_s(r)\rho(r)dr + E_{xc} \tag{3.5}$$

In equation 3.5, E states energy, T_s denotes kinetic energy, J represents Coloumbic energy, υ_s denotes external potential and E_{xc} denotes exchange-correlation energy. Exchange-correlation energy functional does not depend on electron density in KS equation therefore, it cannot be determined directly. Because of this reason, some approximations have been developed to determine exchange-correlation energy such as local density approximation (LDA) or generalized gradient approximation (GGA). For fuel cells, DFT methods have been shown to be highly effective in exploring catalyst alternatives for both anode and cathode reactions.

3.3 Nudged Elastic Band Method

In many chemical phenomena, energy barrier has a key role. Thus, determining the energy barriers on minimum energy paths is a necessity. Minimum energy path (MEP) refers to minimum barrier value between the two local minima on the potential energy surface. NEB method, which developed by Henkelman and Jónsson [39-40], works properly for identifying transition states between initial and final states and reaction barriers that associate with chemical reactions. NEB starts with locating the shortest path between identified two local minima and this path divided by equal parts according to given image number. A spring constant defines between every images and NEB starts interpolating every image for finding MEP on the potential energy surface. Optimization of MEP performed by analysing forces, which are spring forces and perpendicular component of total force on every image.

In Figure 3.1, dashed line is initial path, solid one is MEP on potential energy surface (PES) after NEB operation.

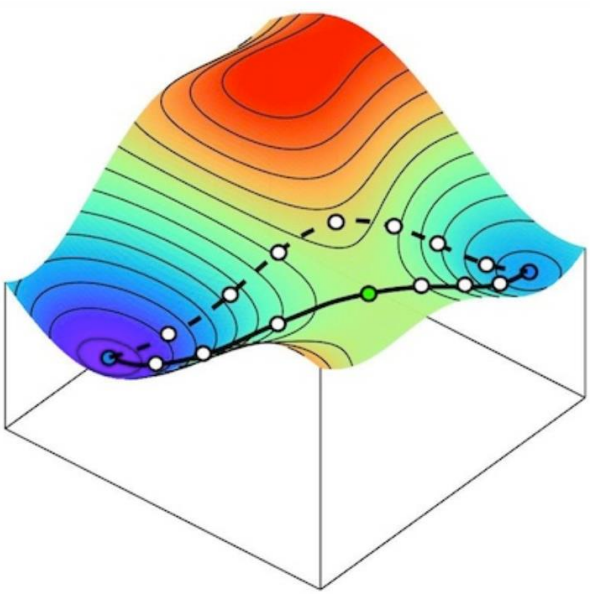

Figure 3.1 : Typical NEB method application demonstration [41].

4. RESULTS AND CONCLUSION

All calculations in this study are performed with generalized gradient approximation DFT with plane-wave basis set and ultrasoft pseudopotentials [42]. A graphene sheet with lattice parameters of a=17.25 Å ve b=14.93 Å are employed. A vacuum area of being 15 Å is applied for minimizing interactions between graphene layers. After the metal binding and formation energy calculations, $N_2S_2V_1$ structure was selected to study the ORR. All NEB and geometry optimization processes are conducted with Quantum Espresso program [43]. $N_2S_2V_1$ structure has 98 atoms when it is undoped. For this study, metallic dopants are determined as Au, Ag, Mn and Pt. In Figure 4.1 undoped $N_2S_2V_1$-graphene is shown. Blue represents nitrogen, yellow is sulphur and gray is for carbon atoms.

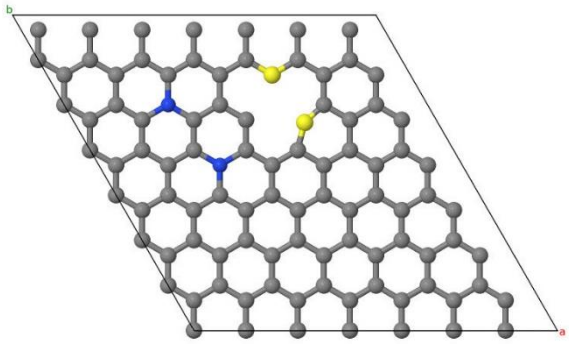

Figure 4.1 : Undoped $N_2S_2V_1$-Graphene.

Finding the minimum energy structure is compulsory for DFT calculations. For increasing the accuracy of analysis different positions of newly added atomic species should be tried for different sites of the surface. For instance, in this study, oxygen is putted on at least ten diffrent positions and optimazition processes are done for each coordinate system on each five different graphene surfaces for finding the minimum oxygen binding energy. This approach is repeated for other reaction steps similarly. Optimization of initial states in hydrogenation steps are also performed including different hydrogen adsorption sites on graphene surface for finding the most appropriate low energy positions.

4.1 MEP Calculations of $N_2S_2V_1$-Graphene

First, the four steps of total ORR is modelled on non-metalic doped structure. Determining of the oxygen molecule's adsorption site on the surface is a compulsory step for starting MEP calculations. Firstly, oxygen molecule is located at different positions on the surface which are considered as possible active sites and then the minimum energy one is selected to carry out the oxygen dissocation step calculations. Comparison of different sites is given in Table 4.1 and Figure 4.2.

Table 4.1 : Total energy and bond lengths of different oxygen adsorption sites on $N_2S_2V_1$-Graphene.

Sites	Energy (Ry)	Bonds	Bond lengths (Å)
a	-1244.35457736	O-O	1.39
		C-O	1.34
b	-1244.26089636	O-O	1.4
		C-O	1.46
c	-1244.38585482	O-O	1.4
		C-O	1.37

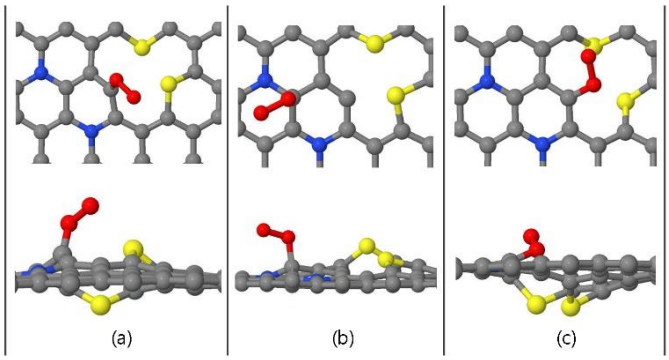

Figure 4.2 : Different sites of oxygen adsorption on $N_2S_2V_1$-Graphene.

Based on these oxygen adsorption calculations, the minimum energy system is site c which is selected to complete oxygen dissocation reaction barrier calculations. In addition to better energy level of the site c, oxygen is positioned very close to structure and relatively bonded strongly with respect to other cases.

Figure 4.3 contains oxygen dissocation reaction barier on NS doped graphene together with initial, transition and final states of reaction, respectively . As it can be seen on Figure 4.3, the reaction barrier is calculated to be 1.493 eV. From initial to final state, oxygen-oxygen bondis broken and oxygen atoms are bonded with different carbon atoms. C-O bonds are shorten from 1.37 Å to 1.25 Å and 1.28 Å, respectively, in the transition and final states. O-O bond length is found to be 1.40 Å in the initial state

and this length is slightly increased to 1.44 Å in the transition state and finally oxygen atoms are well separated with a distance of 2.88 Å.

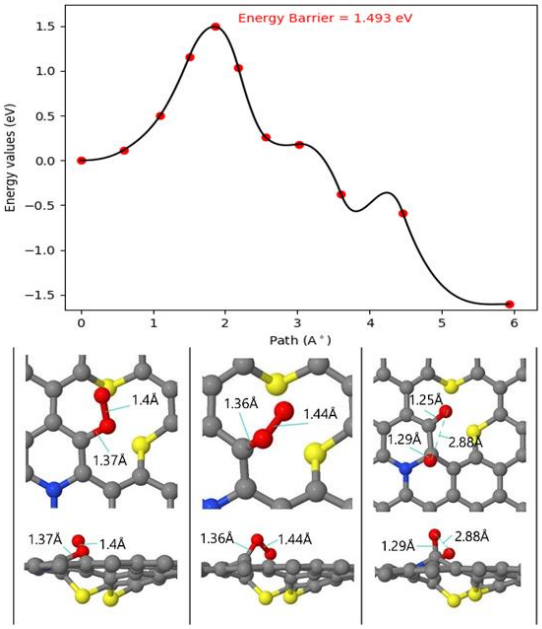

Figure 4.3 : The first reaction step of non-metallic structure.

The first hydrogenation process is the second step of ORR. After that step one of the dissocatiated oxygen takes a hydrogen from the surface and first OH group is formed. Figure 4.4 illustares both reaction barrier and pathway. Reaction barrier of this step is calculated to be 0.145 eV.

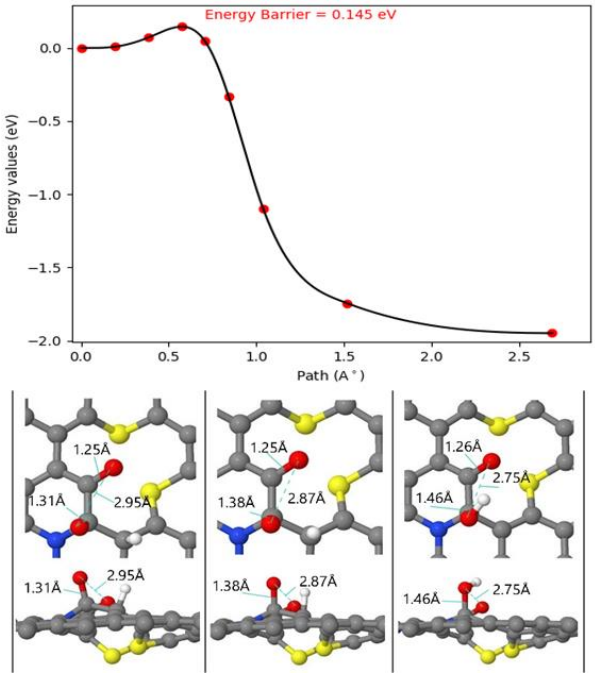

Figure 4.4 : The second reaction step of non-metallic structure.

As it shown clearly in the Figure 4.4, C-O bond in the initial state and C-OH bond which is formed in the final state is elongated from 1.31 Å to 1.46 Å and the distance between *OH group and the other atomic oxygen is getting closer from 2.95 Å to 2.75 Å. In particular, a weak hydrogen bond occurs with a distance of 2.15 Å. The other atomic oxygen is almost remain at the its initial position.

The third step of ORR is the production and removal of the first water molecule. In Figure 4.5 reaction barrier of this reaction step is showed together with the reaction pathway. The reaction barrier of this reaction is calculated to be 0.745 eV.

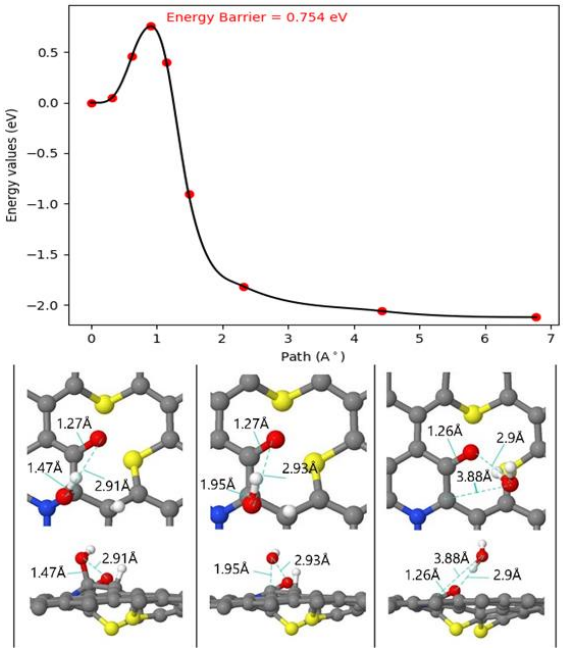

Figure 4.5 : The third reaction step of non-metallic structure.

In the third step of reaction, *OH group breaks its bond with carbon atom and is getting molecular formation. More specifically, C-O bond is elongated from 1.47 Å to 1.95 Å from initial to transition state. After the breaking the C-OH bond, OH group takes the second hydrogen and water molecule is formed at the 3.88 Å away from the other atomic oxygen. It should also be noted that there is a formation of hydrogen bond between the water molecule and the atomic oxygen on the graphene surface with a distance of 2.90 Å.

The fourth step of ORR which is the second OH formation step occurs as shown in Figure 4.6 and the reaction barrier is calculated to be 0.864 eV. At the fourth step of reaction the last oxygen atom takes the hydrogen atom and *OH configuration is formed. At the initial state C-O bond length is 1.26 Å and it is elongated to 1.36 Å

after the OH is formed. This result is similar to the second reaction step: when OH group is formed, C-O bond has become weaken and elongated.

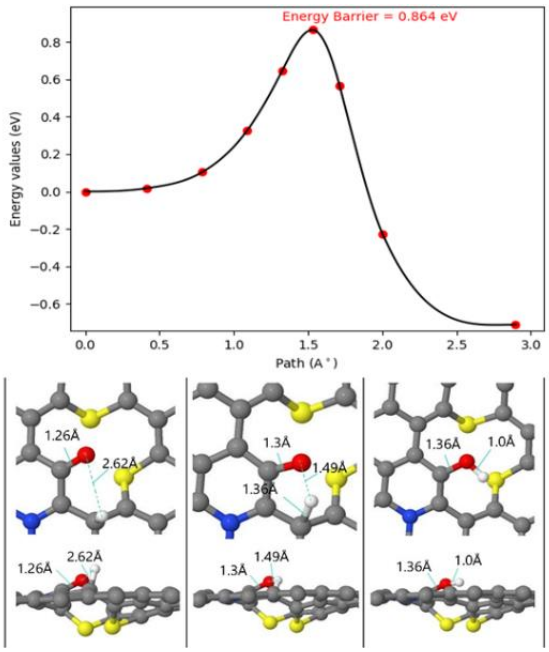

Figure 4.6 : The fourth reaction step of non-metallic structure.

The last step of reaction is modelled but achieved results was not satisfactory due to occurred reaction barriers were very high. Because of this reason, further investigations on the fifth step of the reaction will be conducted.

4.2 MEP Calculations for Ag-$N_2S_2V_1$-Graphene

Before the MEP calculation, first minimum energy oxygen adsorption configuration is determined for Ag-$N_2S_2V_1$ graphene structure. Bonding details and the total energies are given in Table 4.2 and visual demonstration of different adsorption sites are given in Figure 4.7.

Table 4.2 : Total energy and bond lengths of different oxygen adsorption sites on Ag-$N_2S_2V_1$-Graphene.

Sites	Energy (Ry)	Bond	Bond lenghts (Å)
a	-1539.71152691	O-O Ag-O	1.35 2.12
b	-1539.70759155	O-O Ag-O	1.35 2.12
c	-1539.7260214	O-O Ag-O	1.35 2.14

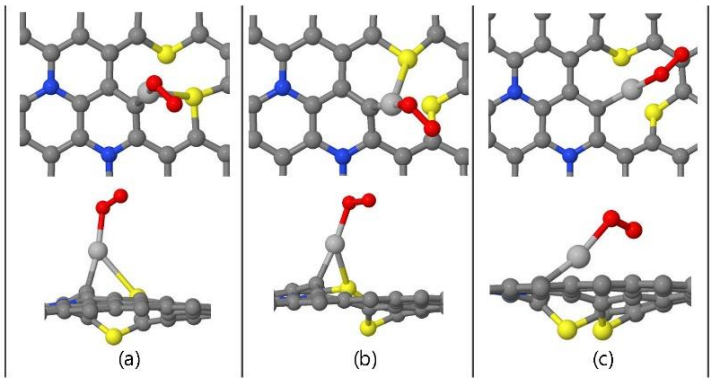

Figure 4.7 : Different sites of oxygen adsorption on Ag- $N_2S_2V_1$-Graphene.

Ag atom binds the oxygen molecule by far away above the graphene surface in all cases. The minimum energy configuration is achieved with site c.

Figure 4.8 represents oxygen dissocation step reaction barrier and initial, transition and final states of the reaction , respectively. As it is shown in Figure 4.8, the reaction barrier is found to be 1.105 eV.

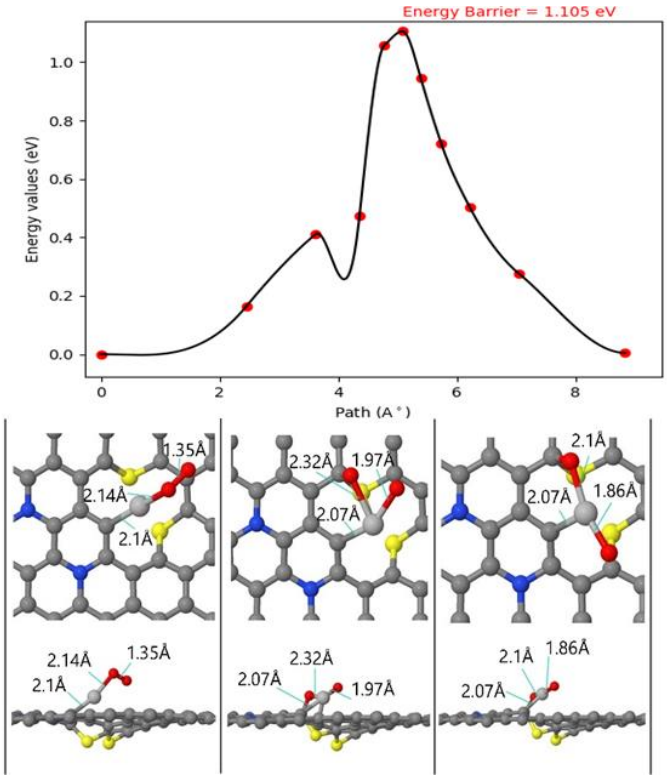

Figure 4.8 : The first reaction step of Ag doped structure.

During this process, oxygen atoms are getting away from each other and one of these forms a bridge configuration between C and Ag in the transition state and this is kept

in the final state. Ag-C bond does not change so much and Ag-O bond lengths are 2.10 Å and 1.86 Å, respectively .

The reaction barrier of the second step is calculated to be 0.157 eV. And here the first OH group is formed . Figure 4.9 illustrates both MEP and important reaction steps.

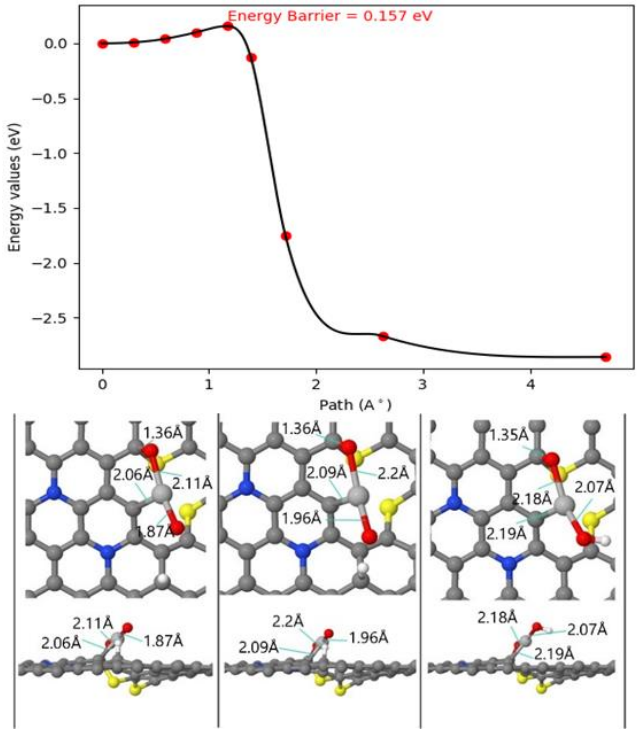

Figure 4.9 : The second reaction step of Ag doped structure.

In the second step of reaction, hydrogen attacks to the oxygen atom which is only bonded to Ag. . This resulted the elongation of bond lenghts around Ag. In particular, Ag-C bond is elongated from 2.06 Å to 2.19 Å, Ag-O bond is elongated from 2.11 Å to 2.18 Å and the Ag-O bond is elongated from 1.87 Å to 2.07 Å.

In Figure 4.10, the reaction barrier of the first water formation and the corresponding initial, final and transition structures of this reaction is illustrated . The reaction barrier is computed to be 0.272 eV. In first water molecule removal step, water molecule leaves the graphene surface and it is located by 3.75 Å away from the Ag atom. Ag-C and remaining O-C bonds are more strengthen. In contrast, remaining Ag-O bond is weakened, in particular it is elongated from 2.15 to 2.25 Å when passing from initial to final state. The bond length of remaining O-C bond is changed from 1.36 Å to 1.28 Å and Ag-C from 2.19 Å to 2.13 Å.

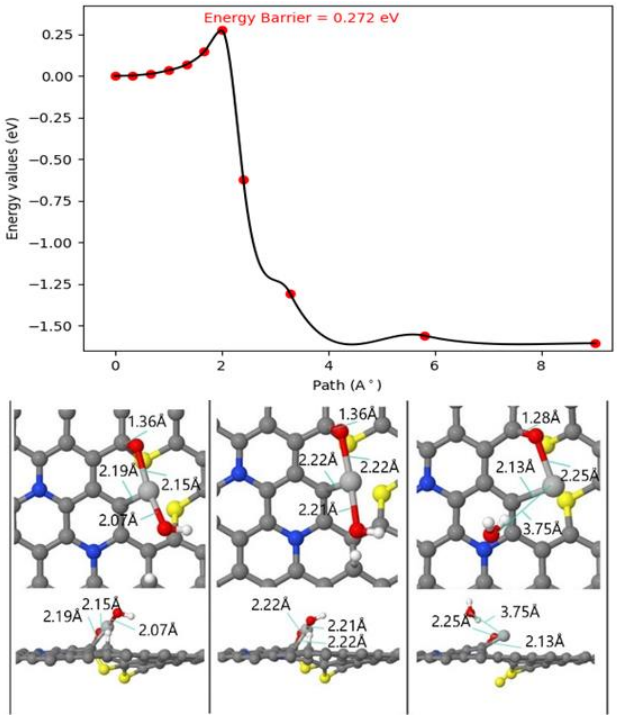

Figure 4.10 : The third reaction step of Ag doped structure.

As shown in Figure 4.11, the last step which is modelled in this study for Ag-$N_2S_2V_1$-graphene is the second hydrogenation step. The calculated energy barrier is 0.504 eV for this reaction and which is almost 0.40 eV higher than the metal-free case.

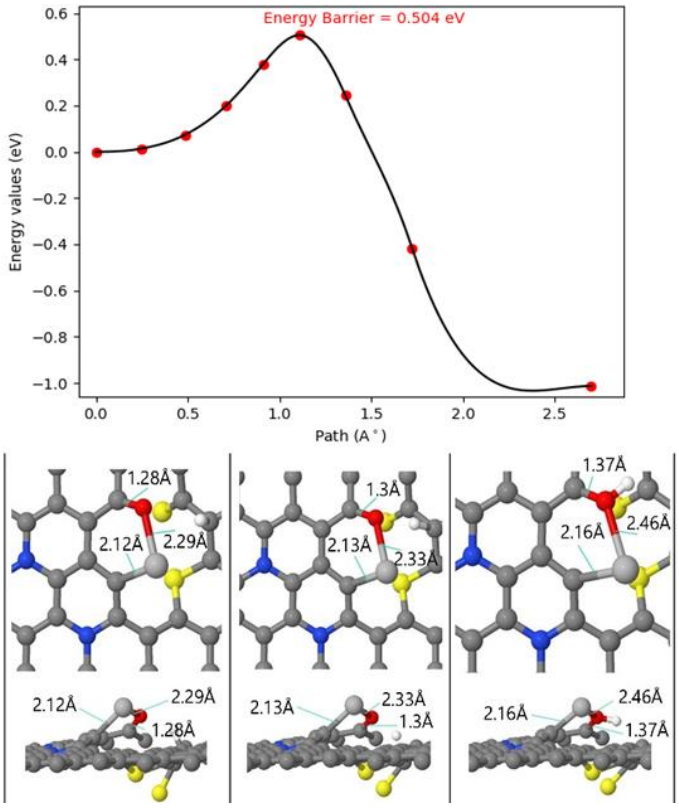

Figure 4.11 : The fourth reaction step of Ag doped structure.

In this step, between initial and final states all Ag related bonds are increased. In particular, O-C bond length is elongated form 1.28 Å to 1.37 Å, Ag-O bond length is elongated from 2.29 Å to 2.46 Å and Ag-C bond is elongated from 2.12 Å to 2.16 Å.

Fifth reaction step was modelled. However, achieved MEP graphics were not proper for representing in the thesis.

4.3 MEP Calculations for Au-$N_2S_2V_1$-Graphene

At the beginning of the MEP calculation standard procedure is applied to Au-$N_2S_2V_1$-graphene structure as similar to other cases . Oxygen molecule is located on the different sites on the structure and lowest energy configuration is selected to model the ORR steps. Table 4.3 and Figure 4.12 contains details about the oxygen adsorption process.

Table 4.3 : Total energy and bond length of different oxygen adsorption sites on Au-$N_2S_2V_1$-Graphene.

Sites	Energy (Ry)	Bond	Bond lengths (Å)
a	-1518.33006861	O-O Au-O	1.35 2.07
b	-1518.31138252	O-O Au-O	1.35 2.07
c	-1518.23986928	O-O C-O	1.38 1.51

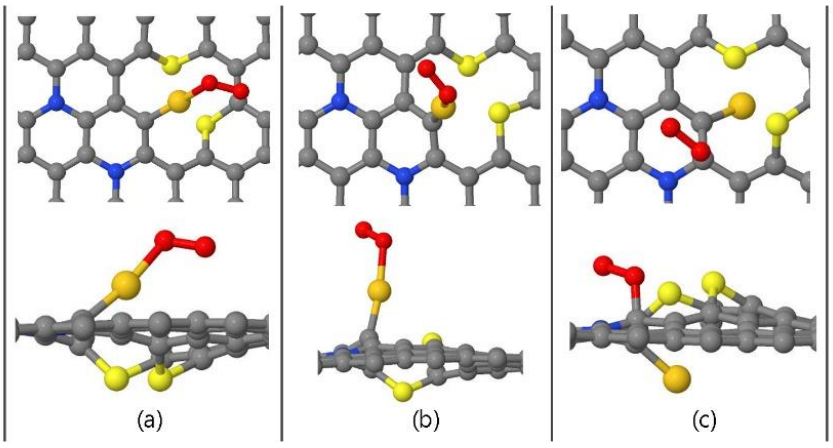

Figure 4.12 : Different sites of oxygen adsorption on Au-$N_2S_2V_1$-Graphene.

In this structure oxygen molecule is mostly adsorbed on the Au atom. However, another active site is also found near the metal atom and here oxygen molecule adsorbed on the graphene surface also binds to a C atom on the surface. When the

results are considered, a site is found more favorable energitically and therefore this configuration is choosen for the subsequent MEP calculations.

In Figure 4.13, details of the first step of reaction are given. The energy barrier of first step is 1.26 eV.

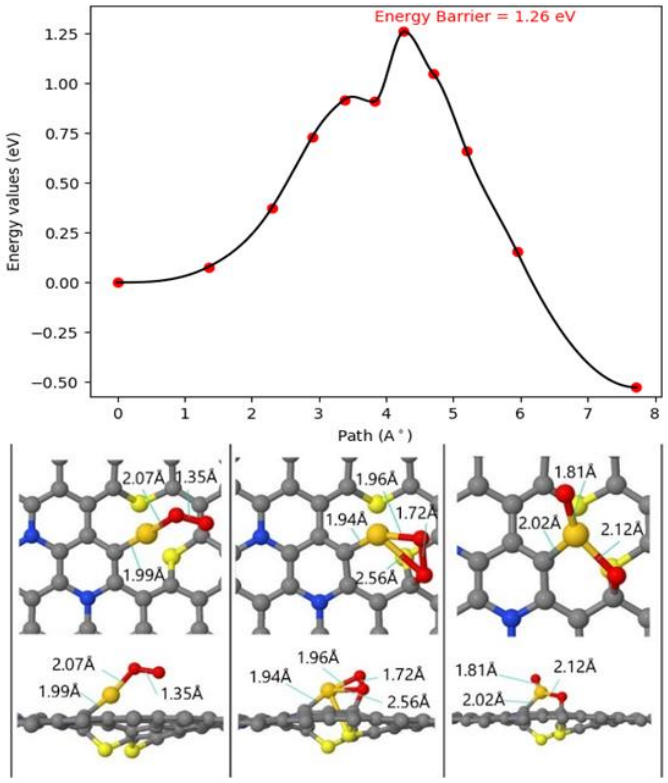

Figure 4.13 : The first reaction step of Au doped structure.

In oxygen dissocation step of Au-$N_2S_2V_1$-graphene structure, oxygen molecule on Ag forms a bridge with the graphene surface at the transition state. In the final state of the reaction, one of the oxygen is bonded with both Au and C atoms. The other oxygen atom is only bonded with Au atom and it is more free than the other the oxygen atom. Au-C bond length is slightly differed during the reaction: it is differed from 1.99 Å to 2.02 Å.

For the second step of ORR, a reaction barrier of 0.022 eV is found as shown in Figure 4.14. In the second step of the reaction, Au atom elongates its C bond between initial and final states. Au-C bond length is increased from 2.0 Å to 2.11 Å. On the other hand, the bond between Au and oxygen atom, which takes hydrogen atom, is weakened . In particular, the Au-O bond length is changed dramatically from 1.81 Å to 2.0 Å. There is no a notable difference in the bond distances between the remaining oxygen atom and Au.

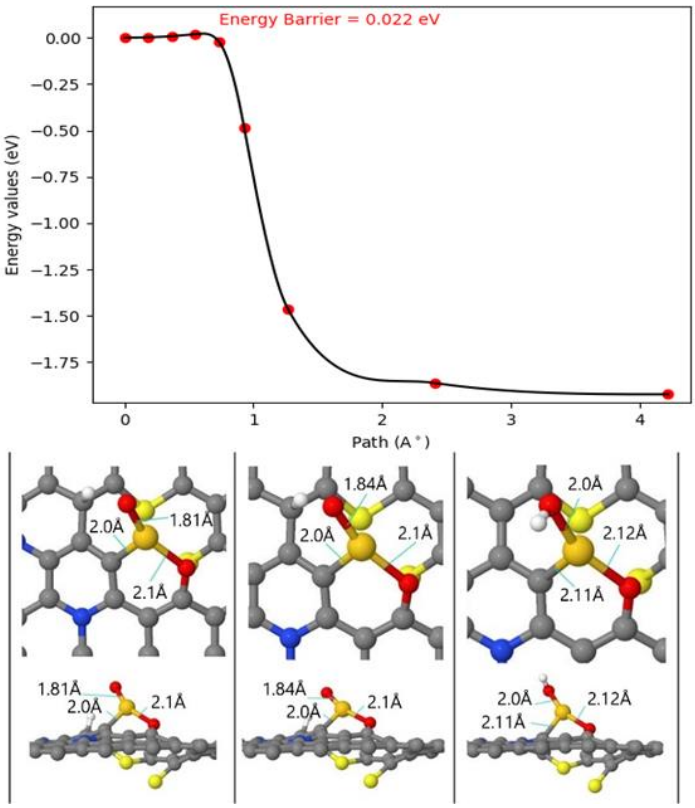

Figure 4.14 : The second reaction step of Au doped structure.

In Figure 4.15, the third reaction barrier and the corresponding initial, transition and final states of the reaction are represented. The reaction barrier is calculated only to be 0.159 eV.

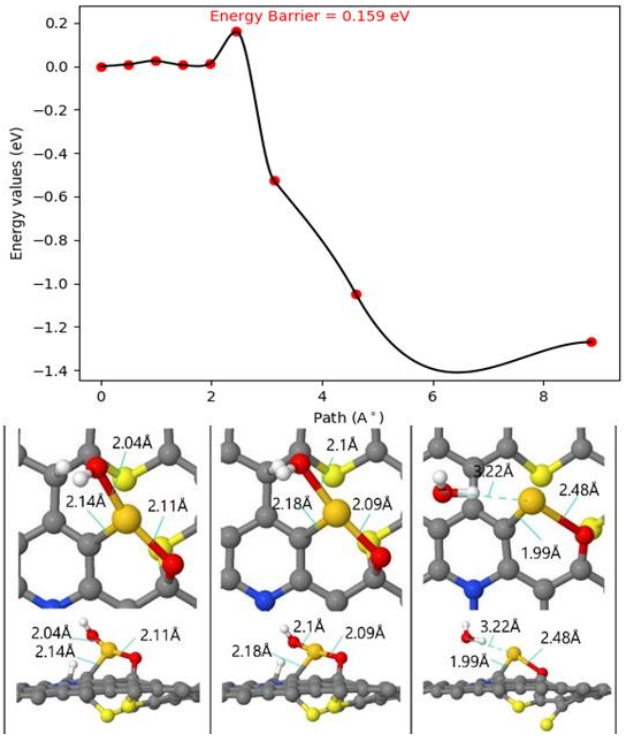

Figure 4.15 : The third reaction step of Au doped structure.

In the first water removal step, water molecule which is removed from the graphene surface is positioned 3.22 Å away from Au atom in the final state.The bond between Au and the remaining oxygen atom is weakened by an elongation from 2.11 Å to 2.48 Å. Lastly, Au atom is got closer to the graphene surface and its bond length with C atom is changed from 2.14 Å to 1.99 Å in the final state.

The fourth step of ORR is the second hydrogenation step. Figure 4.16 represents the details of this step. The barrier of this reaction is calculated to be 0.673 eV.

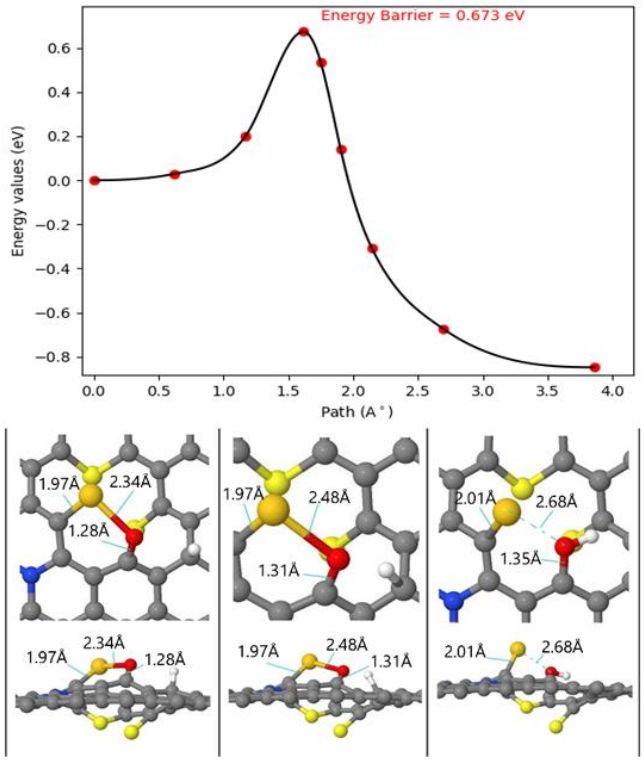

Figure 4.16 : The fourth reaction step of Au doped structure.

In the second hydrogenation step of reaction, OH is formed at the final state. OH formation causes the breaking of Au-O bond. O-C bond is elongated from 1.28 Å to 1.35 Å. Distance between oxygen and Au atom is differed from 2.34 Å to 2.68 Å.

The last step of ORR and its details are given in Figure 4.17. For the removal of the second water an energy of 0.855 eV is required.At the final step, hydrogenated OH group is bonded with Au atom at the transition state. It is clear that in the previous step Au-O bond was broken but, after the optimization with second hydrogen atom Au-O

bond is re-established. At the final state water molecule is located 3.24 Å away from Au atom and Au-C bond length is slightly increased.

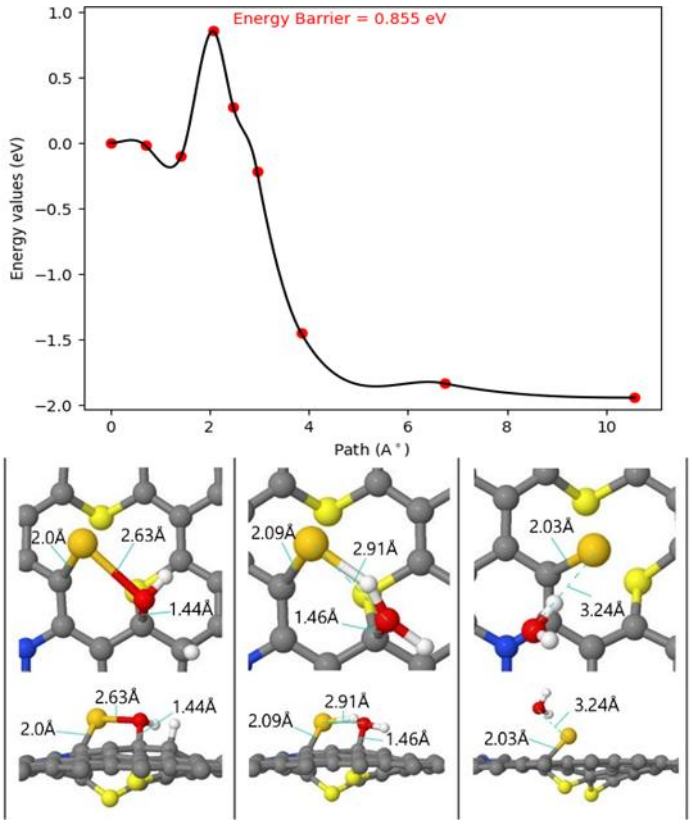

Figure 4.17 : The fifth reaction step for Au doped structure.

4.4 MEP Calculations for Mn-$N_2S_2V_1$-Graphene

Different adsorption sites of molecular oxygen on Mn-$N_2S_2V_1$-graphene is first investigated. The resulting energies and configurations are listed and shown in Table 4.4 and Figure 4.18.

Table 4.4 : Total energy and bond length of different oxygen adsorption sites on Mn-$N_2S_2V_1$-Graphene.

Sites	Energy (Ry)	Bond	Bond lengths (Å)
a	-1530.35671434	O-O	1.39
		Mn-O	2
		Mn-O	1.74
b	-1530.36754526	O-O	1.44
		Mn-O	2.04
		Mn-O	1.68
c	-1530.07037783	O-O	1.34
		S-O	2.02

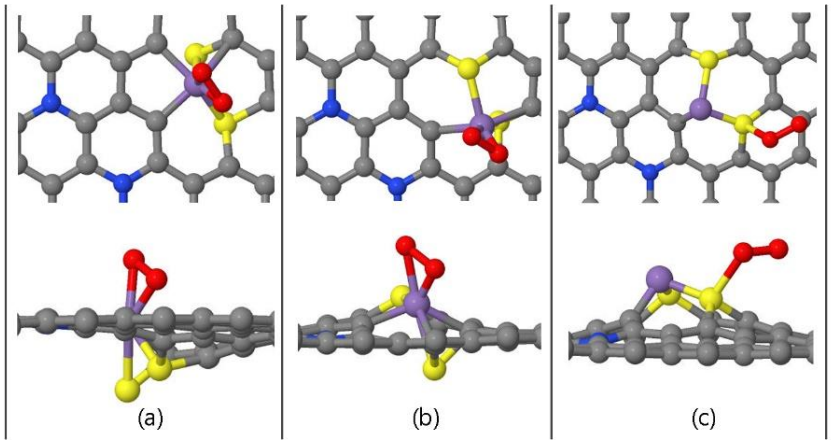

Figure 4.18 : Different sites of oxygen adsorption on Mn-$N_2S_2V_1$-Graphene.

Oxygen is mostly adsorbed on Mn atom. However, in site c oxygen is bonded with one of the S atoms. Both a and b site oxygen is formed bridge configuration on Mn atom. For the MEP calculations b site configuration is selected due to its lowest total energy.

The first studied reaction is the dissociation of oxygen and as shown in Figure 4.19 a barrier of 1.059 eV is required for this reaction step.

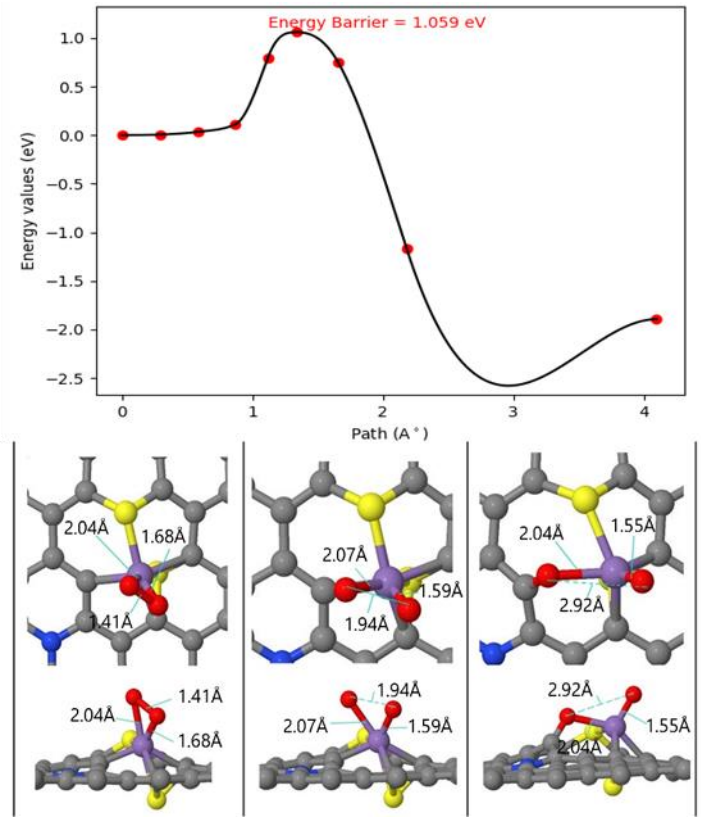

Figure 4.19 : The first reaction step of Mn doped structure.

In the first step of the reaction, O-O bond is broken at the transition step and one of the oxygen is bonded with C atom of the graphene surface and the other one remains only bonded to Mn atom. The distance between oxygen atoms is differs from 1.41 Å to 2.92 Å.

In Mn doped case only two reaction steps are investigated so far. The second step considered for Mn is the fourth step of ORR. As shown in Figure 4.20, the barrier height for this reaction is obtained to be 0.125 eV.

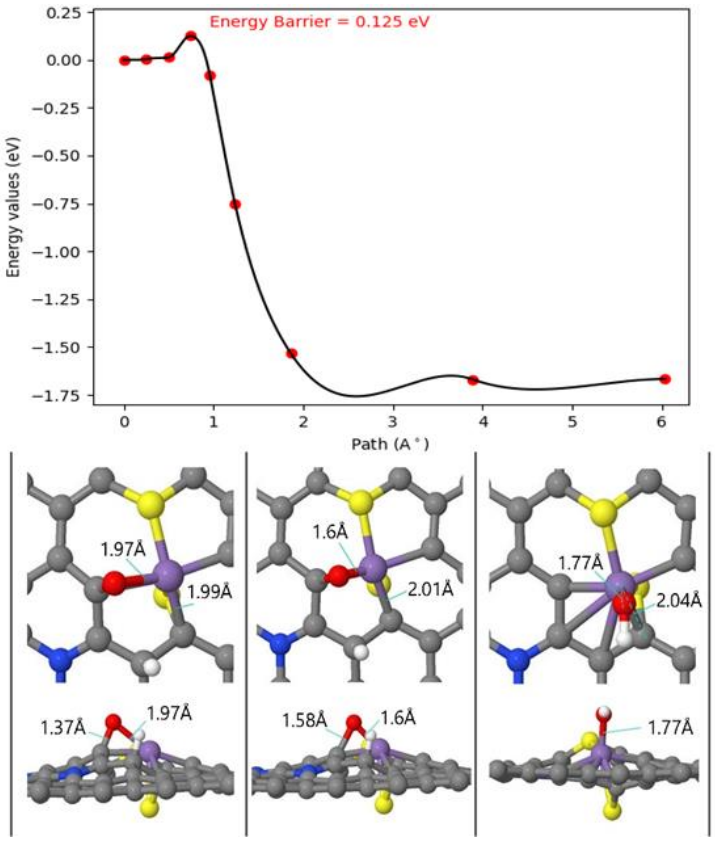

Figure 4.20 : The fourth reaction step of Mn doped structure.

In the fourth step of total reaction, bridge configuration of oxygen is broken and then OH group is formed and bonded only to Mn atom. Mn-O bond length is shortened from 1.97 Å to 1.77 Å. Mn-C bond is slightly increased between initial and final states.

Third and fifth reaction steps were investigated. However, water molecule was mostly bonded on Mn atom instead of leaving the structure. Because of this reason, results of third and fifth reactions are not presented in the thesis.

4.5 MEP Calculations for Pt-$N_2S_2V_1$-Graphene

Table 4.5 and Figure 4.21 indicate the energy and configuration of different molecular adsorption sites on the Pt-$N_2S_2V_1$-graphene surface.

Table 4.5 : Total energy and bond length of different oxygen adsorption sites on Pt-$N_2S_2V_1$-Graphene.

Sites	Energy (Ry)	Bond	Bond lengths (Å)
a	-2242.01214328	O-O Pt-O	1.33 2.12
b	-2242.0234722	O-O Pt-O	1.35 2.12
c	-2242.03730482	O-O Pt-O	1.34 2.11

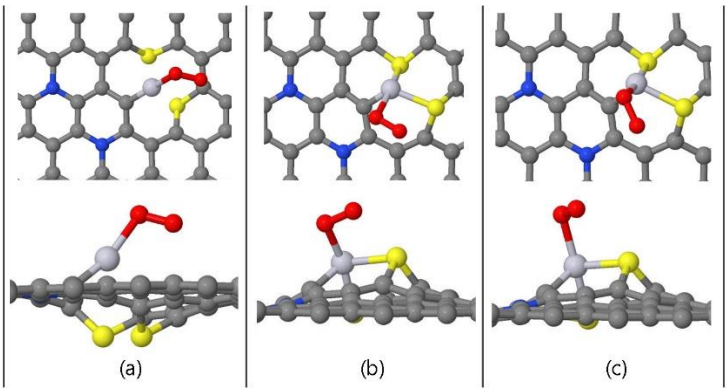

Figure 4.21 : Different sites of oxygen adsorption on Pt-$N_2S_2V_1$-Graphene.

Oxygen is mostly adsorbed on Pt atom. In Pt-$N_2S_2V_1$-graphene surface case firstly c site configuration selected for the subsequent barrier energy calculations. However, the first barrier calculation (dissociation of oxygen molecule) on c site configuration shows that the reaction occurs endothermically. This result is not favorable for oxygen dissociation reaction. Then, b site selected for calculations, but the achieved result was similar to c site's result. Thus, a site configuration is selected to perform MEP calculations and exothermic reaction characteristic is achieved.

As shown in Figure 4.22, to dissociate oxygen on Pt an energy of 1.09 eV is required. Similar to Au doped surface one of the oxygen atoms is bonded with C atom after the dissociation and the other one is located at a freer position. From initial to final state, Pt-C bond is elongated. The first length of Pt-C bond is 1.81 Å, at the end of the reaction Pt-C bond length becomes 2.12 Å.

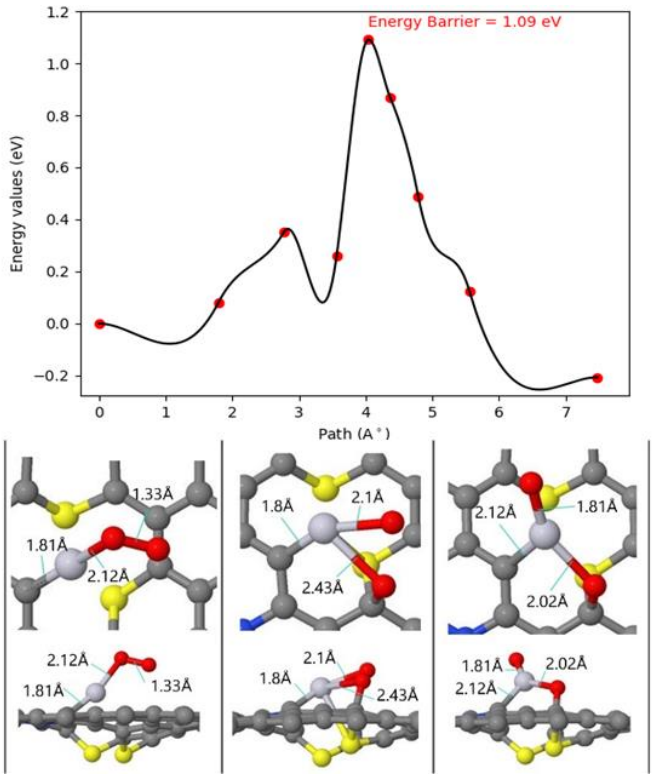

Figure 4.22 : The first reaction step of Pt doped structure.

For the formation of first *OH, only an energy of 0.086 eV is required as shown in Figure 4.23.

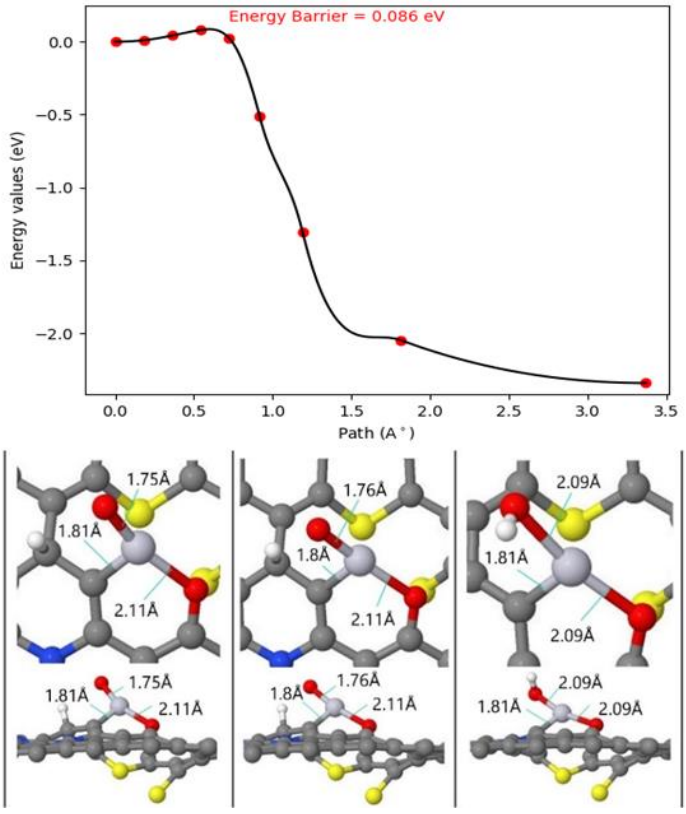

Figure 4.23 : The second reaction step of Pt doped structure.

In the first hydrogenation step, one of the oxygen atoms takes the hydrogen atom and the bond length is elongated from 1.75 Å to 2.09 Å. The position of Pt and the other oxygen atom is not much differed. Because of the relatively small movement of atomic species, reaction barrier is very low in this step.

For the third step (formation of the first water molecule) of ORR, a barrier with 0.349 eV is found as shown in Figure 4.24.

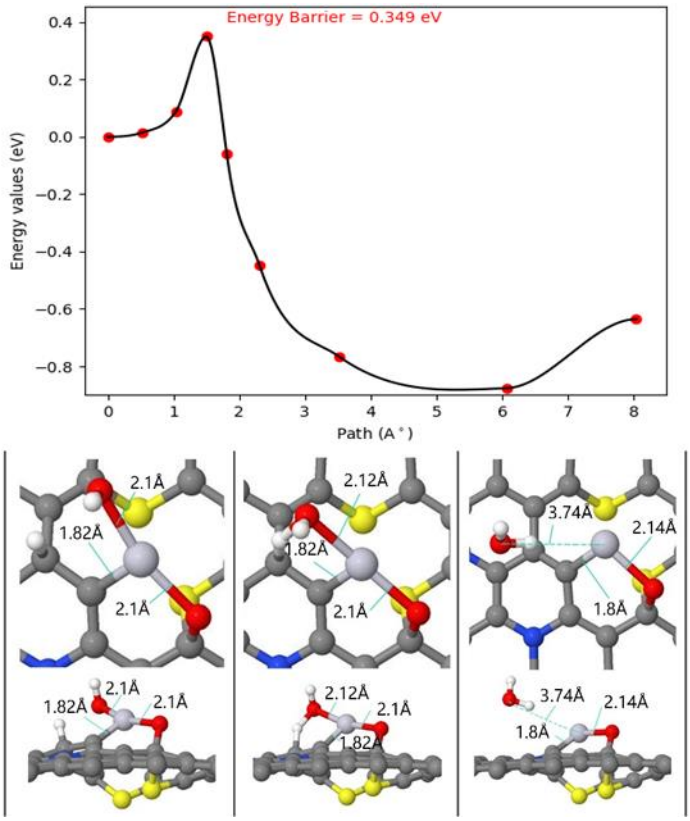

Figure 4.24 : The third reaction step of Pt doped structure.

In the first water removal step, water molecule is located 3.74 Å away from Pt atom at the final state. Pt-C and Pt-O bonds are showed small difference in terms of bond length between the initial and final states. Pt atom gets closer to the graphene surface when passing from the initial to final state .

The last investigated reaction step is actually the fourth step (formation of the second *OH) in Pt doped structure. The reaction barrier is obtained to be 0.637 eV as shown in Figure 4.25. In the second hydrogenation step on the graphene surface, Pt-O bond is elongated from 2.13 Å to 2.45 Å. Pt-C bond length is almost the same in both initial and final states.

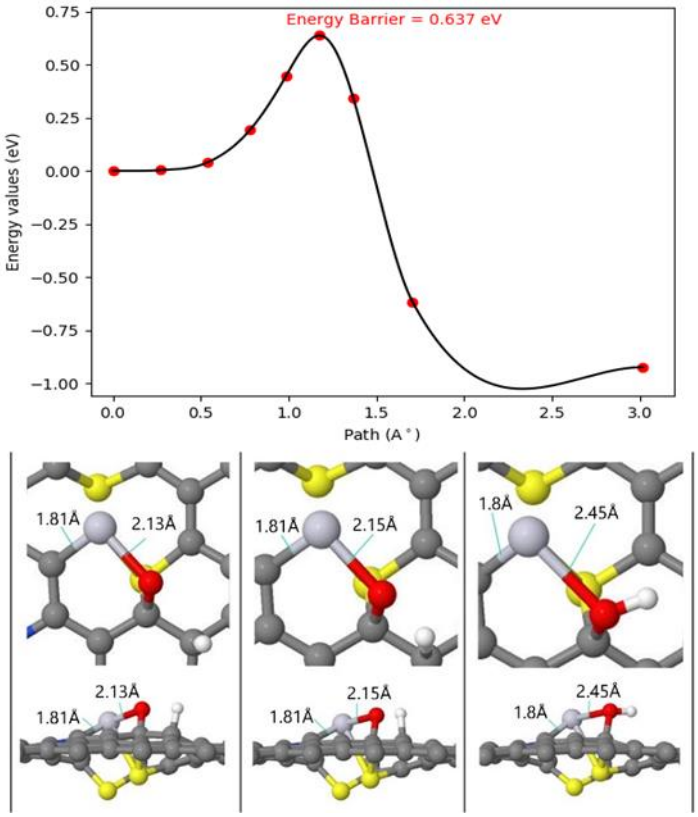

Figure 4.25 : The fourth reaction step of Pt doped structure.

The last reaction step on the Pt doped surface was investigated. Relatively high barrier values and unproper MEP graphics are achieved. Because of this reason, results are not presented on the thesis.

4.6 Discussion

MEP calculations shows that metal doping has a positive effect on the ORR as it has been already mentioned in the literature for different catalytic reactions. Reaction barriers which belong to non-metal doped graphene are higher than metallic doped ones. The highest barriers are obtained in the oxygen dissocation step at all considered systems as similar to the literature. In Pt, Au and Ag doped graphene surfaces one of the dissociated oxygens is bound with only metal atom. This oxygen atom takes hydrogen easier than the other oxygen atom. Actually, comparison of reaction barriers between the second and the third steps highligths this fact. After the removal of the more free oxygen, the hydrogenation step of the other oxygen (fourth step) becomes harder and thus reaction barriers are getting higher than the barriers of the second step. In comparison to previously mentioned literature results, oxygen dissociation

performance of non-metalic doped $N_2S_2V_1$ is slightly better. In contrast to non-metalic doped graphene, the metalic doped ones have a better performance from the previous literature results.

REFERENCES

[1] **Wang, J., Wang, H. and Fan Y.** (2018). Techno-Economic challenges of fuel cell commercialization, *Engineering*, Vol: 4, no. 3, pp. 352-360.

[2] **Novoselov K. S., Geim A. K., Morozov S. V., Jiang D., Zhang1 Y., Dubonos S. V., Grigorieva I. V and Firsov A. A.** (2004). Electric field effect in atomically thin carbon films, *Science*, Vol: 306, no. 5696, pp. 666-669.

[3] **Fazio, G., Ferrighi, L., Perilli, D. and Valentin, C. D.** (2016). Computational electrochemistry of doped graphene as electrocatalytic material in fuel cells, *International Journal of Quantum Chemistry*, Vol: 116, no. 22, pp. 1623-1640.

[4] **Lee W. J., Maiti U. N., Lee J. M., Lim J., Han T. H. and Kim S. O.** (2014). Nitrogen-doped carbon nanotubes and graphene composite structures for energy and catalytic applications, *Chem. Commun*., 50, 6818.

[5] **Qu, L., Liu, Y., Baek J. and Dai L.** (2010). Nitrogen-Doped Graphene as Efficient Metal-Free Electrocatalyst for Oxygen Reduction in Fuel Cells, *ACS Nano*, 4, 3, 1321-1326.

[6] **Zhang, L., and Xia, Z.** (2011). Mechanisms of Oxygen Reduction Reaction on Nitrogen-Doped Graphene for Fuel Cells, *J. Phys. Chem. C*,115,22,11170-11176.

[7] **Yang, Z., Yao, Z., Li, G., Fang, G., Nie, H., Liu, Z., Zhou, X., Chen, X. and Huang, S.** (2012). Sulfur-doped graphene as an efficient metal-free cathode catalyst for oxygen reduction, *ACS Nano*,6,1,205-211.

[8] **Fazio, G., Ferrighi, L. and Valentin, C.** (2014). Boron-doped graphene as active electrocatalyst for oxygen reduction reaction at a fuel-cell cathode, *Journal of Catalysis*,318,203-210.

[9] **Li, R., Wei, Z., Gou, X. and Xu, W.** (2013). Phosphorus-doped graphene nanosheets as efficient metal-free oxygen reduction electrocatalysts, *RSC Adv.*, 3, 9978-9984.

[10] **Li, M., Zhang, L., Xu, Q., Niu, J. and Xia, Z.** (2014). N-doped graphene as catalysts for oxygen reduction and oxygen evolution reactions: Theoretical considerations, *Journal of Catalysis*,314,66-72.

[11] **Jiao, Y., Zheng, Y., Jaroniec, M. and Qiao, S. Z.** (2014). Origin of the electrocatalytic oxygen reduction activity of graphene-based catalysts: A roadmap to achieve the best performance, *J. Am. Chem. Soc.*, 136, 4394−4403.

[12] **Chen, X., Chen, S. and Wang, J.** (2016). Screening of catalytic oxygen reduction reaction activity of metal-doped graphene by density functional theory, *Applied Surface Science*,379,291-295.

[13] **Toh, R. J, Poh, H. L., Sofer, Z. and Pumera, M.** (2013). Transition Metal (Mn, Fe, Co, Ni)-Doped Graphene Hybrids for Electrocatalysis,*Chem. Asian J.*, 8, 1295 – 1300.

[14] **Stolbov, S. and Ortigoza, M. A.** (2015). Gold-doped graphene: A highly stable and active electrocatalysts for the oxygen reduction reaction, *J. Chem. Phys.*, 142, 154703.

[15] **Xu, H., Cheng, D., Cao, D. and Zheng, X. C.** (2018). A universal principle for a rational design of single-atom electrocatalysts, *Nature Catalysis*, 1,339-348.

[16] **Lv, Y., Yang, L. and Cao, D.** (2019). Sulfur, Nitrogen and Fluorine Triple-Doped Metal-Free Carbon Electrocatalysts for the Oxygen Reduction Reaction, *ChemElectroChem*, 6, 741 – 747.

[17] **Razmjooei, F., Singh, K. P., Song, M. Y. and Yu, J.** (2014). Enhanced electrocatalytic activity due to additional phosphorous doping in nitrogen and sulfur-doped graphene: A comprehensive study, *Carbon*, 78, 257-267.

[18] **Byon, H. R., Suntivich, J. and Shao-Horn, Y.** (2011). Graphene-Based Non-Noble-Metal Catalysts for Oxygen Reduction Reaction in Acid, *Chem. Mater.*, 23, 3421–3428.

[19] **He, Y., Tan, Q., Lu, L., Sokolowski, J. and Wu, G.** (2019). Metal-Nitrogen-Carbon Catalysts for Oxygen Reduction in PEM Fuel Cells: Self-Template Synthesis Approach to Enhancing Catalytic Activity and Stability, *Electrochemical Energy Reviews*, 2,231–251.

[20] **Asefa, T.** (2019). Metal-free and noble metal-free heteroatom-doped nanostructured carbons as prospective sustainable electrocatalysts, *Acc. Chem. Res*.,49,9,1873-1883.

[21] **Tang, C. and Zhang, Q.** (2017). Nanocarbon for Oxygen Reduction Electrocatalysis: Dopants, Edges, and Defects, *Adv. Mater*., 1604103.

[22] **Jiang, H., Gu, J., Zheng, X., Liu, M., Qiu, X., Wang, L., Li, W., Chen, Z., Ji, X. and Li, J.** (2019). Defect-rich and ultrathin N doped carbon nanosheets as advanced trifunctional metal-free electrocatalysts for the ORR, OER and HER, *Energy Environ. Sci.*, 12, 322-333.

[23] **Zheng, Y., Xiao, W., Cho, M. and Cho, K.** (2013). Density functional theory calculations for the oxygen dissociation on nitrogen and transition metal doped graphenes, *Chemical Physics Letters*, 586, 104–107.

[24] **Yang, M., Wang, L., Li, M., Hou, T. and Youyong, L.** (2015). Structural stability and O2 dissociation on nitrogen-doped graphene with transition metal atoms embedded: A first-principles study, *AIP ADVANCES*, 5, 067136.

[25] **Blomen, L. J. M. J. and Mugerwa, M. N.** (1993). *Fuel Cell Systems. New York*, NY.: Springer-Science.

[26] **Perry, M. L. and Fuller, T. F.** (2002). A Historical Perspective of Fuel Cell Technology in the 20th Century, *Journal of The Electrochemical Society*, 149,7,59-67.

[27] **Andujar, J. M. and Segura, F.** (2009). Fuel cells: History and updating. A walk along two centuries, *Renewable and Sustainable Energy Reviews*, 13, 2309–2322.

[28] **Dicks, A. L. and Rand, D. A. J.** (2018). *Fuel Cell Systems Explained (3rd ed.). New Jersey*, NJ.: John Wiley & Sons, Inc.

[29] **Url-1** *<https://airandspace.si.edu/collection-objects/fuel-cell-gemini-cutaway>*, date retrieved 10.06.2019

[30] **Url-2** *<https://airandspace.si.edu/collection-objects/fuel-cell-apollo>*, date retrieved 10.06.2019

[31] **Verspagen, B.** (2007). Mapping Technological Trajectories as Patent Citation Networks: A Study on The History of Fuel Cell Research, *Advances in Complex Systems*, Vol. 10, No. 1, 93–115.

32] **Xu, Q., Gu, X. and Feng, Y.** (2014). Knowledge Adaptability Evaluation in View of Patent Citation in Technological Evolutionary Process: A Case Study of Fuel Cell, *International Journal of Software Engineering and Knowledge Engineering,* Vol. 25, No. 8, 1335–1364.

[33] **Behling, N. H.** (2013). *Fuel Cells: Current Technology Challenges and Future Research Needs.* San Diego, CA.: Elsevier

[34] **Dai, L., Chang, D. W., Baek, J. and Lu, W.** (2012). Carbon Nanomaterials for Advanced Energy Conversion and Storage. *Small* ,8, 8, 1130–1166.

[35] **O'hayre, R., Cha, S., Colella, W. G. and Prinz, F. B.** (2016). *Fuel Cell Fundamentals (3rd ed.).* New Jersey, NJ.: Wiley.

[36] **Stacy, J., Regmi, Y. N., Leonard, B. and Fan, M.** (2016). The recent progress and future of oxygen reduction reaction catalysis: A review. *Renewable and Sustainable Energy Reviews,* 69, 401–414.

[37] **Hohenberg, P. and Kohn, W.** (1964). Inhomogeneous electron gas, *Physical review*, 136 (3B), B864.

[38] **Kohn, W. and Sham, L. J.** (1965). Self Consistent Equations Including Exchange and Correlation Effects, *Physical review*, 140, A1133.

[39] **Jónsson, H., Mills, G., Jacobsen, K., W.** (1998) Nudged Elastic Band Method for Finding Minimum Energy Paths of Transitions, in Classical and Quantum Dynamics in Condensed Phase Simulations, *World Scientific*,385.

[40] **Henkelman, G. and Jónsson, H.** (2000) Improved Tangent Estimate in the NEB method for Finding Minimum Energy Paths and Saddle Points, *J. Chem. Phys.*, 113, 9978.

[41] **Url-3** *<http://umet.univ-lille1.fr/Projets/RheoMan/en/to-learn-more about/nudged-elastic-band.php>*, date retrieved 10.06.2019

[42] **Vanderbilt, D.** (1990). Soft self-consistent pseudopotentials in a generalized eigenvalue formalism, *Phys. Rev. B*, 41, 7892.

[43] **Giannozzi, P., Baroni, S., Bonini, N., Calandra, M., Car, R., Cavazzoni, C., Ceresoli, D., Chiarotti, G. L., Cococcioni, M., Dabo, I. et al.** (2009). QUANTUM ESPRESSO: a modular and open-source software project for quantum simulations of materials. Journal of Physics: Condensed Matter, 21(39), 395502.

CURRICULUM VITAE

Name Surname **:** Hasan Ozan AVCI

E-Mail **:** hasan.ozan.avci@gmail.com

EDUCATION :

B.Sc. : 2016, Yıldız Technical University, Faculty of Mechanical Engineering, Department of Mechanical Engineering

PROFESSIONAL EXPERIENCE AND REWARDS:

- 12.2018 - Still – Ankara University – Research Assistant – Department of Energy Engineering